Am J Physiol Cell Physiol 308: C123–C138, 2015.
First published October 29, 2014; doi:10.1152/ajpcell.00090.2014.

Deletion of small ankyrin 1 (sAnk1) isoforms results in structural and functional alterations in aging skeletal muscle fibers

E. Giacomello,[1,6]* M. Quarta,[2]* C. Paolini,[3,6] R. Squecco,[4,6] P. Fusco,[1] L. Toniolo,[2,6] B. Blaauw,[2,6,8] L. Formoso,[1] D. Rossi,[1,6] C. Birkenmeier,[5] L. L. Peters,[5] F. Francini,[4,6] F. Protasi,[3,6] C. Reggiani,[2,6,7]† and V. Sorrentino[1,6]†

[1]*Molecular Medicine Section, Department of Molecular and Developmental Medicine, University of Siena, Siena, Italy;* [2]*Department of Biomedical Sciences, University of Padova, Padua, Italy;* [3]*Ce.S.I., Center for Research on Ageing and Department of Neuroscience, Imaging, and Clinical Sciences, University G. d'Annunzio, Chieti, Italy;* [4]*Department of Experimental and Clinical Medicine, University of Florence, Florence Italy;* [5]*Jackson Laboratory, Bar Harbor, Maine;* [6]*IIM-Interuniversity Institute of Myology;* [7]*CNR-Neuroscience Institute, Padua, Italy; and* [8]*Venetian Institute of Molecular Medicine, Padua, Italy*

Submitted 24 March 2014; accepted in final form 26 October 2014

Giacomello E, Quarta M, Paolini C, Squecco R, Fusco P, Toniolo L, Blaauw B, Formoso L, Rossi D, Birkenmeier C, Peters LL, Francini F, Protasi F, Reggiani C, Sorrentino V. Deletion of small ankyrin 1 (sAnk1) isoforms results in structural and functional alterations in aging skeletal muscle fibers. *Am J Physiol Cell Physiol* 308: C123–C138, 2015. First published October 29, 2014; doi:10.1152/ajpcell.00090.2014.—Muscle-specific ankyrins 1 (sAnk1) are a group of small ankyrin 1 isoforms, of which sAnk1.5 is the most abundant. sAnk1 are localized in the sarcoplasmic reticulum (SR) membrane from where they interact with obscurin, a myofibrillar protein. This interaction appears to contribute to stabilize the SR close to the myofibrils. Here we report the structural and functional characterization of skeletal muscles from sAnk1 knockout mice (KO). Deletion of sAnk1 did not change the expression and localization of SR proteins in 4- to 6-mo-old sAnk1 KO mice. Structurally, the main modification observed in skeletal muscles of adult sAnk1 KO mice (4–6 mo of age) was the reduction of SR volume at the sarcomere A band level. With increasing age (at 12–15 mo of age) extensor digitorum longus (EDL) skeletal muscles of sAnk1 KO mice develop prematurely large tubular aggregates, whereas diaphragm undergoes significant structural damage. Parallel functional studies revealed specific changes in the contractile performance of muscles from sAnk1 KO mice and a reduced exercise tolerance in an endurance test on treadmill compared with control mice. Moreover, reduced Q_γ charge and L-type Ca^{2+} current, which are indexes of affected excitation-contraction coupling, were observed in diaphragm fibers from 12- to 15-mo-old mice, but not in other skeletal muscles from sAnk1 KO mice. Altogether, these findings show that the ablation of sAnk1, by altering the organization of the SR, renders skeletal muscles susceptible to undergo structural and functional alterations more evident with age, and point to an important contribution of sAnk1 to the maintenance of the longitudinal SR architecture.

aging; ankyrins; excitation-contraction coupling; myopathy; sarcoplasmic reticulum

THE SARCOPLASMIC RETICULUM (SR) of skeletal muscle is a specialized form of endoplasmic reticulum that is involved in Ca^{2+} storage, release, and reuptake. Consequently, the SR is a main player in regulating muscle contraction as it allows a rapid release of Ca^{2+} induced by membrane depolarization in a process named excitation-contraction (e-c) coupling. In skeletal muscle, e-c coupling occurs at specialized intracellular junctions, named triads, where two terminal cisternae of the SR are positioned to flank, on opposite sites, a transverse (T)-tubule (17). To efficiently position the Ca^{2+} store close to the contractile apparatus, the SR is organized to surround each individual myofibril in a specific relationship that is a prerequisite for its function (17). Accordingly, in mammalian skeletal muscle, the junctional SR, where the ryanodine receptor Ca^{2+} release channels are positioned, is localized at the transition between A and I bands of the sarcomere, so that each sarcomere has two sites of Ca^{2+} release along its length, whereas the longitudinal SR, mainly responsible for Ca^{2+} uptake, is distributed around the A and I bands of the sarcomere. Although the importance of intracellular organization of the SR is essential for supporting the mechanisms of e-c coupling, at present, the mechanisms underlying the formation and maintenance of the highly organized structure of the SR and its relationship with the sarcomere striation in skeletal muscle cells are still poorly understood (16, 39, 45).

In the past years, a group of small muscle-specific transcripts of the *Ank1* gene (sAnk1) have been identified (8, 20, 21). These transcripts encode different small muscle-specific ankyrin isoforms named sAnk1.5, sAnk1.6, sAnk1.7, sAnk1.8, and sAnk1.9, of which sAnk1.5 is the most abundant. In contrast with canonical ankyrins, sAnk1 isoforms lack both membrane and spectrin-binding domains, but contain a unique NH_2-terminal amino acid sequence that contains a hydrophobic domain, which anchors these proteins to the SR membranes (3, 4, 7, 50). The most abundant isoform, sAnk1.5, is expressed from the early stages of skeletal muscle development, and in mature muscle fibers sAnk1.5 is preferentially localized at the level of the M-band and, to a lesser extent, at the Z-disk (22).

Several studies reported that sAnk1.5 is able to bind to obscurin, a myofibril-associated protein (3, 4, 27). Obscurin is a giant muscle protein known to bind titin and myomesin, and proposed to play an important role in the assembly of myofibrils, especially at the level of the M-band (19, 26, 49). Obscurin has a modular architecture characterized by multiple Ig-like domains, FN(II)-like domains, a Rho-GEF, and a pleckstrin-like domain followed by a nonmodular COOH-terminal region that contains two binding sites for muscle-specific

* E. Giacomello and M. Quarta contributed equally to this work.
† C. Reggiani and V. Sorrentino contributed equally to this work.

Address for reprint requests and other correspondence: V. Sorrentino, Molecular Medicine Section, Dept. of Molecular and Developmental Medicine, Univ. of Siena, Siena, Italy (e-mail: vincenzo.sorrentino@unisi.it).

ankyrins including sAnk1.5 (3, 4, 27), ankB (13, 36) and ankG107 (25, 30). Different isoforms of obscurin of variable length are generated by either alternative splicing or usage of an internal promoter resulting in the inclusion of a COOH-terminal exon that encodes two serine/threonine kinase motifs (18).

Localization of obscurin at the surface of myofibrils (27, 49) together with evidence that it can interact with sAnk1.5 localized on the SR initially led to the suggestion that these two proteins may have a role in maintaining a stable connection between the myofibrils and the SR (4, 27). In this context, work by Lange and collaborators (28) showed that loss of obscurin in skeletal muscle did not affect sarcomere organization and alignment, and had no dramatic influence on the junctional SR morphology. Nevertheless, skeletal muscles from obscurin KO mice did display changes in the architecture of the longitudinal SR. In fact, obscurin KO skeletal muscle showed a deficiency of longitudinal SR membranes likely due to a defective anchorage between SR membranes and the contractile cytoskeleton. Moreover, obscurin KO muscles displayed lower levels of sAnk1.5 protein, probably due to protein degradation caused by the lack of its natural interactor. Interestingly, after the age of 12 mo, obscurin KO muscles show centrally localized nuclei, indicating the development of a myopathy with age. In addition, work from our laboratory has demonstrated that obscurin KO mice also present alterations in the organization of dystrophin at costameres, likely the result of mislocalization of ankB in the subsarcolemmal region (36).

In a recent study, the role of sAnk1 in skeletal muscle was directly examined by siRNA knockdown in isolated muscle fibers (1). Partial knockdown of sAnk1 was accompanied by changes in the levels of SERCA and sarcolipin, two proteins localized on the longitudinal SR, but did not significantly alter the expression of triadic proteins. Fibers deficient in sAnk1.5 had a longitudinal SR reduced in size and characterized by a less developed network of tubules that were in part swollen. In parallel, these authors also showed that fibers where sAnk1 was knocked down had an altered Ca^{2+} homeostasis since there was a reduced release of Ca^{2+} and a slow reuptake from the SR probably due to SERCA reduction (1).

The role of sAnk1.5 in connecting SR membranes and the contractile apparatus is further supported by studies on a mouse model, *Tmod1*$^{-/-Tg+}$ mice, where tropomodulin 1 is selectively depleted in skeletal muscles tissue (24). In this work, sAnk1.5 was shown to directly interact with Tmod3 in a multiprotein complex localized at the M-band in complex with γ-cyto-actin, Tm4, and Tm5NM1. Interestingly, in the absence of Tmod1, Tmod3 localization at the M-line was lost, causing sAnk1.5 mislocalization at the Z-line. These observations were accompanied by evident changes in the SR morphology that presented swelling phenomena, and in the SR functionality that displayed a defective Ca^{2+} release.

Despite the above-mentioned observations, direct evidence for the role of sAnk1 isoforms and the consequence of their loss in muscle physiology are still unclear. To answer these questions, we generated sAnk1 KO mice, and here we report the results of a morphological and functional characterization of this mouse model. The results indicate that knockout of sAnk1 induces morphological and functional alterations in skeletal muscles, which appear to worsen with age and to affect more severely the diaphragm muscle.

MATERIALS AND METHODS

Animal Treatment

All experiments followed the official guidelines laid down by the European Community Council (directive 86/609/EEC) incorporated into Italian Government Legislation. Experiments have been performed with the approval by the Local Ethical Committee and from Ministero della Salute, Rome, Italy. In addition, animal treatment for experiments conducted at the Jackson Laboratory followed the Association for Assessment and Accreditation of Laboratory Animal Care (AAALAC) specifications. In the experiments reported in this manuscript two groups of mice of different age were used. The first group consists of mice of 4–6 mo of age, referred to as young mice; the second group consists of mice of 12–15 mo of age, referred to as old mice.

Antibodies

The antibodies utilized in immunofluorescence and Western blot experiments are the following: anti-ank1.5 (3), anti-obscurin (4), anti-RyR1 (23), anti-SERCA-1 (clone CaF2-5D2, Developmental Studies Hybridoma Bank), anti-triadin (Trisk-95, kindly provided by Dr. I. Marty), anti-calsequestrin-1 and -2 (purchased from ABR, Golden, CO), anti-α1s-DHPR (clone 1A, purchased from Abcam, Cambridge, MA), anti-JP1 (Invitrogen, Carlsbad, CA), anti-JP2 (Invitrogen), anti β-tubulin (clone B-5-1-2, Sigma, St Louis, MO), and anti-α-actinin (clone EA-53, Sigma).

Gene Targeting

Mouse Ank1 genomic clones were isolated from a 129/SvλFixII library (Stratagene, La Jolla, CA) using standard techniques (40). Detailed restriction maps were prepared and a targeting construct designed to replace Exon 39a with a neomycin-resistance cassette was generated in the pPNT vector (40). A 4.1-kb upstream *Stu*I/*Xho*I arm containing Exon 39 was blunt end ligated into the *Xba*I site of the vector and a 2.6-kb downstream *Bcl*I/*Bgl*II arm containing exons 40 and 41 into the *Xho*I site (Fig. 1*A*). Electroporated 129/Sv-J1 embryonic stem (ES) cells were cultured and selected with G418 and gancyclovir (47). ES cell DNA was isolated, digested with *Sst*I/*Xba*I, and analyzed by Southern blot using a 5′ flanking 2.8-kb *Stu*I fragment as a probe. The correctly targeted alleles were detected as a 9.8-kb band and the wild-type allele as a 9.0-kb band (Fig. 1*B*). Correctly targeted clones were injected into C57BL/6J blastocysts and embryo transfer performed by the Jackson Laboratory Cell Biology and Microinjection Service. Male chimeras were mated to C57BL/6J females to select for germ line transmission. Animals for this study were derived by backcrossing to C57BL/6J for 10 generations and then intercrossing to produce homozygous KO/KO animals and +/+ siblings for controls. Progeny genotyping was done by the polymerase chain reaction (PCR) using forward primer 5′-CAGAGACA-CAAAACGTAGCC coupled with reverse primer 5′-TCTATCGC-CTTCTTGACGAG (NEO) for the KO allele and reverse primer 5′-TTCTCATTCTCCTCTCCGAC for the normal allele. Total cellular RNA from hindlimb skeletal muscle was prepared using Trizol reagent (Invitrogen, Carlsbad, CA). Northern and Southern blots were performed according to Sambrook and Russell (40).

Preparation of Samples for Immunofluorescence Experiments

Muscles [diaphragm, extensor digitorum longus (EDL), tibialis anterior, and soleus] were dissected from at least three sAnk1 KO and three control B6 mice of 4–6 mo (young mice) and of 12–15 mo of age (old mice). Samples were then frozen in liquid nitrogen and cryoprotected with Tissue-Tek II OCT compound (Sakura Finetek Europe, Leiden, The Netherlands). Transverse or longitudinal sections 8 μm thick were cut with a Leica cryostat (CM 1850, Leica Microsystem, Wetzlar, Germany) and fixed with 3% paraformaldehyde.

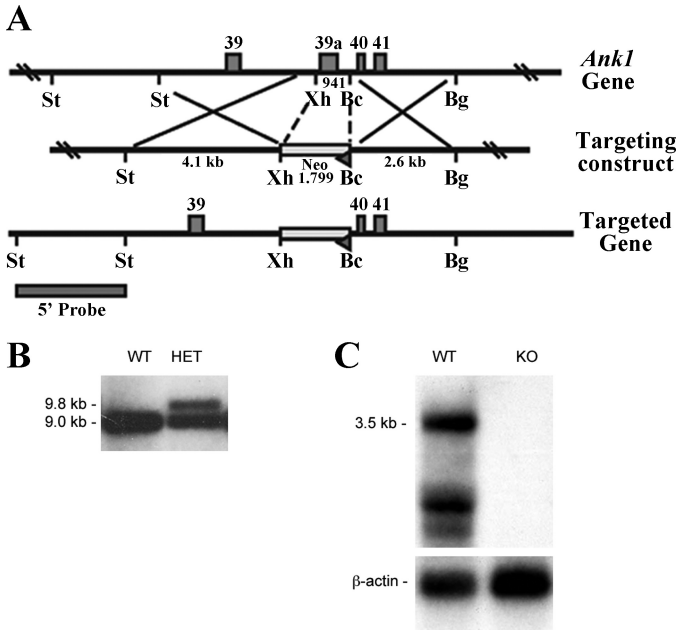

Fig. 1. Schematic representation of specific knockout of muscle-specific small ankyrins 1 (sAnk1). Exon 39a was replaced by a DNA segment containing a Neo cassette (*A*). Southern blot (*B*) was performed with the 5′ flanking probe drawn in *A*, confirming the insertion of the Neo cassette in genomic DNA of sAnk1 knockout (KO) mice. Northern blot on skeletal muscle total cellular RNA (*C*), using a probe recognizing the skeletal muscle-specific first exon, identifies sAnk1 transcripts in wild type (WT; *left lane*) but not in KO (*right lane*). St, *Stu*I; Xh, *Xho*I; Bc, *Bcl*I; Bg, *Bgl*II; HET, heterozygote.

Sections were then blocked with 0.2% BSA and 5% goat serum in PBS to avoid nonspecific binding of the antibodies, and incubated with primary antibodies overnight. The sections were extensively washed with PBS-BSA 0.2% and incubated with Cy2 or Cy3 conjugated secondary antibodies (Jackson ImmunoResearch Laboratories, Lexington, KY) for 1 h, at the recommended concentration, at room temperature, washed with PBS-BSA 0.2% and mounted with Mowiol added with 0.025% DABCO (Sigma) as antifading agent. The specimens were analyzed with a confocal laser scan microscope (LSM510, Zeiss, Jena, Germany) equipped with an inverted microscope (Axiovert 200, Zeiss).

Evans Blue Dye Test

The 12- to 15-mo-old sAnk1 WT and KO mice ($n = 7$) were injected with 50 μl of a 10 mg/ml Evans Blue dye solution per 10 g body weight, into the peritoneal cavity as previously described (46). The following day mice were killed by cervical dislocation; diaphragm muscles were frozen in liquid nitrogen and sectioned as reported above. Transversal sections were mounted with Mowiol and analyzed with an epifluorescent microscope (Axiovert, Zeiss). The percentage of positive fibers was established by calculating the ratio between Evans Blue dye positive and total fibers.

Preparation of Samples for Histology and Electron Microscopy (EM)

Diaphragm and EDL muscles were carefully dissected from WT and sAnk1 KO male mice at two different ages: 4–6 and 12–15 mo. Muscles were fixed at room temperature (RT) in 3.5% glutaraldehyde in 0.1 M sodium cacodylate buffer, pH 7.2, for 2 h and kept in fixative until further use. Small bundles of fixed fibers were postfixed and embedded as described in Paolini et al. (34). For histological analysis, longitudinal and cross-oriented semithin sections (250 nm) were cut with a Leica Ultracut R microtome (Leica Microsystem, Wetzlar, Germany) using a Diatome diamond knife (Diatome CH-2501, Biel, Switzerland). After staining with toluidine blue dye, the sections were viewed on a Leica DMLB fluorescence microscope (Leica Microsystem). For EM, ultrathin sections were cut (~50 nm) and, after staining in 4% uranyl acetate and lead citrate, examined with a Morgagni Series 268D electron microscope (FEI, Brno, Czech Republic), equipped with a Megaview III digital camera.

Quantitative Analyses of Histological and EM Specimens

Determination of the number of fibers presenting TAs or contractures in EDL and diaphragm muscles from 12- to 15-mo-old mice were performed on longitudinally oriented semithin sections (histological analysis) stained with toluidine blue dye. Individual fibers were visually scored for the presence of TAs or contractures. The number of fibers with alterations was presented as a percentage of all fibers evaluated, and results of this analysis are reported (see Tables 2 and 3; no. of animals tested = 3 for each group; no. of EDL fibers analyzed for the presence of TAs = 88; no. of diaphragm fibers analyzed for the presence of contractures = 112). SR volume was determined respectively in cross sections of EDL fibers from adult (4–6 mo of age) and ageing (12–15 mo) WT and sAnk1 KO mice using the well-established stereology point-counting techniques (29, 32) in EM micrographs taken at 22,000× magnification after superimposing to the electron micrographs an orthogonal array of dots at a spacing of 0.20 μm. The ratio between numbers of dots falling within the SR profile and the total number of dots covering the whole image was used to calculate the relative volume of fiber occupied by the SR (no. of WT and sAnk1 KO animals tested = 2 + 2; no. of fibers analyzed in each mouse = 5).

SDS PAGE and Immunoblotting

Muscles (diaphragm, EDL, and soleus) from 4- to 6-mo-old or 12- to 15-mo-old mice were carefully dissected and homogenized in RIPA buffer (50 mM Tris-HCl pH 7.4, 150 mM NaCl, 1 mM EDTA, 0.25% Na deoxycholate, 1% NP40) supplemented with protease inhibitor cocktail (Sigma), 1 mM PMSF, 1 mM Na_3VO_4, 1 mM NaF, using TissueRuptor (Qiagen, Hilden, Germany) and lysed for 60 min at 4°C. Insoluble material was removed by centrifugation at 10,000 *g* for 10 min at 4°C, and soluble protein concentration was measured by Bradford quantification assay, in accordance with the manufacturer's instructions (Bio-Rad, Hercules, CA). Protein samples were boiled in Laemmli sample buffer (62.5 mM Tris-HCl, pH 6.8, 10% glycerol, 2% SDS, 0.004% bromophenol blue, 5% β-mercaptoethanol) for 5 min at 95°C before loading. The samples were separated on a polyacrylamide gel electrophoresis in the presence of SDS, according to the standard protocol. Generally, Tris-glycine gels with a 7% resolving gel and a 4% staking gel were used, according to protein size. Samples were run on the gels at constant current of 25 mA in running buffer (10% Tris-glycine, 0.1% SDS). Proteins were electrophoretically transferred onto nitrocellulose or PVDF membranes (Millipore, Billerica, MA) for 1 h at 400 mA. Membranes were then blocked for 1 h in TBST (20 mM Tris, 150 mM NaCl, 0.1% Tween-20, pH 7.4) supplemented with 5% nonfat dry milk and incubated overnight at 4°C with specific primary antibodies. After extensive washings and incubation for 1 h at room temperature with secondary antibodies conjugated with horseradish peroxidase (GE-Healthcare, Little Chalfont, UK), immunoreactivity was analyzed by means of the chemiluminescence detection system (GE-Healthcare, Little Chalfont, UK). ImageJ free software (http://imagej.nih.gov/ij/) was exploited for quantifying the intensities of immunoreactive bands from at least three independent experiments where three animals for each age group (4–6 or 12–15 mo old) were used. Sample loading was normalized to anti-β-tubulin. The differences between treated and control samples are reported as percentage change of sAnk1 KO compared with WT muscles.

Analysis of Ex Vivo Muscle Contractile Performance

Diaphragm, EDL, and soleus muscles were dissected from WT and sAnk1 KO mice of 4–6 or 12–15 mo of age, immersed in warm oxygenated Krebs solution, mounted in a myograph (Muscle Tester System, SI, Heidelberg, Germany) equipped with a force transducer (SI H KG7B, SI, Heidelberg, Germany) and micromanipulator-controlled shaft in a small chamber where oxygenated Krebs solution was continuously circulating. Temperature was kept constant at 25°C. The stimulation conditions were optimized and muscle length was increased until force development during tetanus was maximal. The responses to a single stimulus (twitch) or to a series of stimuli at various rates producing unfused or fused tetani were recorded. Time to peak tension, time to half relaxation, and peak tension were measured in single twitches. Tension was measured in completely fused maximal isometric tetani (for further details see Ref. 34). A minimum of 6 and up to 10 sAnk1 KO and WT mice were used for each single experiment.

Analysis of In Vivo Muscle Contractile Performance

In vivo gastrocnemius mechanics. Gastrocnemius muscle contractile performance was measured in vivo using a 305B muscle lever system (Aurora Scientific, Aurora, ON, Canada) in mice anaesthetized with a mixture of Xylotine and Zoletil. Mice were placed on a thermostatically controlled table, the knee was kept stationary, and the foot was firmly fixed to a footplate, which was connected to the shaft of the motor. Contraction was elicited by electrical stimulation of the sciatic nerve. Teflon-coated 7 multistranded steel wires (AS 632, Cooner Sales, Chatsworth, CA) were implanted with sutures on either side of the sciatic nerve proximally to the knee before its branching. At the distal ends of the two wires the insulation was removed, while the proximal ends were connected to a stimulator (Grass S88). In order to avoid recruitment of the dorsal flexor muscles, the common peroneal nerve was cut. The torque developed during isometric contractions was measured at stepwise increasing stimulation frequency, with pauses of at least 30 s between stimuli to avoid effects due to fatigue. Duration of the trains never exceeded 600 ms. Force developed by plantar flexor muscles was calculated by dividing torque by the lever arm length (taken as 2.1 mm).

Grip test and treadmill endurance test. Strength developed by WT and sAnk1 KO mice during instinctive grasp was measured with the protocol indicated as grip test (12). The mouse was held by the tail in proximity to a trapeze bar connected with the shaft of a force transducer. Once the mouse had firmly grabbed the trapeze, a gentle pull was exerted on the tail. The measurement of the peak force generated by the mouse was repeated several times with appropriate intervals to avoid fatigue, and average peak force values were expressed relative to body mass (12). Endurance was measured with a test to exhaustion on treadmill. Camera settings, lighting, and treadmill speed were set prior to introduction of the mouse. The animal was placed into the testing chamber and the treadmill was turned on. Initial speed (5 cm/s) was increased after 2 min at 10 cm/s. The speed was then increased by 2 cm/s every minute up to 50 cm/s, and time to exhaustion was recorded.

Current- and Voltage-Clamp Experiments

Membrane potential was recorded in current-clamp condition by a microelectrode inserted into single fibers of an isolated muscle bundle of fibers placed on a coverslip and fixed slight stretched at about 120% of the resting length. The passive properties of the sarcolemma, the intramembrane charge movement, ICM, and DHPR/L-type Ca^{2+} current (I_{Ca}) were evaluated in isolated fiber segments using the double Vaseline-gap method in voltage-clamp as previously described (14, 15). All experiments were performed at 22°C. The solutions used were as those employed by Francini et al. (14). All chemicals were obtained from Sigma, except for TEA-OH and 9-anthracene carboxylic acid (Aldrich-Chemie, Steinheim, Germany).

Stimulation and Recording

Digital-to-analog and analog-to-digital conversions were carried out by a Digidata 1200 computer interface (Axon Instruments, Burlingame, CA). Stimulation protocols, data acquisition, and recordings were performed by means of pCLAMP programs, version 6.02 (Axon Instruments). The stability of fibers lasted 150–240 min. The sampling interval was 50 μs. The physiological state of the fibers was evaluated by determining *1*) the resting membrane potential (RMP) in current-clamp, *2*) the membrane capacitance (C_m), as an index of the cell membrane surface, and the specific sarcolemma membrane conductance (G_m/C_m) in voltage-clamp condition. C_m and G_m/C_m were considered as index of membrane stiffness (42) and these two parameters together with RMP as an index of membrane integrity (41). C_m and G_m/C_m were evaluated by applying a voltage pulse of ±10 mV from a holding potential of −80 mV. For I_{Ca} recording, the fibers were held at −80 mV and then 5-s voltage pulses

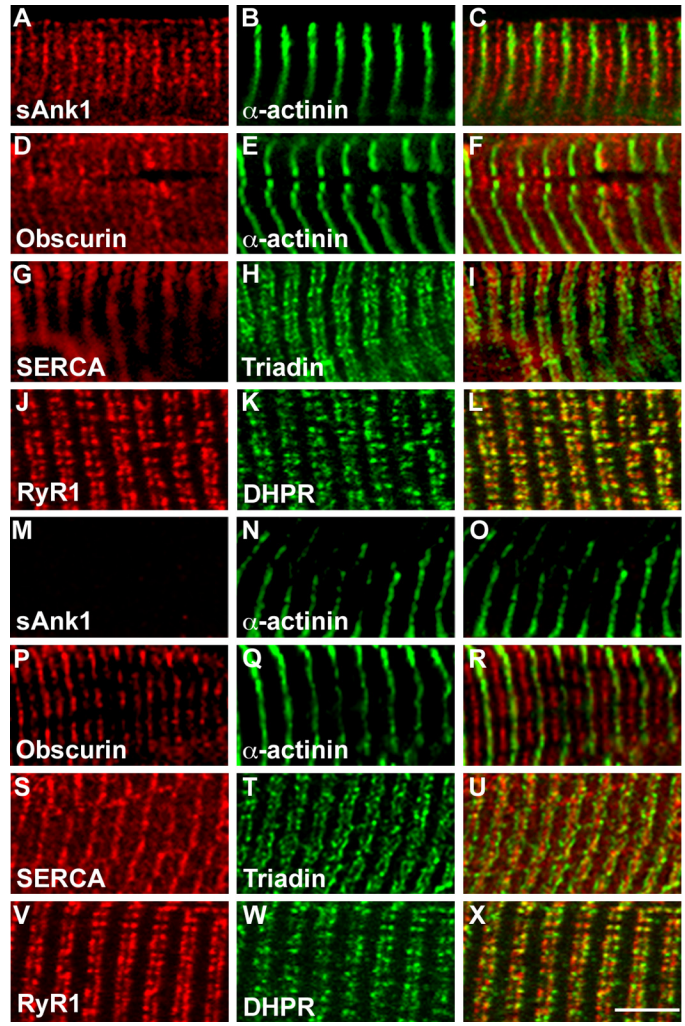

Fig. 2. Extensor digitorum longus (EDL) muscles from 4- to 6-mo-old sAnk1 KO mice do not show altered organization of sarcoplasmic reticulum (SR) and T-tubule proteins. Longitudinal cryosections of 4- to 6-mo-old WT (*A–L*) and sAnk1 KO (*M–X*) EDL were immunolabeled with antibodies against ank1.5 (*A* and *C*; and *M* and *O*), α-actinin (*B, C, E*, and *F*; and *N, O, Q*, and *R*), obscurin (*D* and *F*; and *P* and *R*), SERCA1 (*G* and *I*; and *S* and *U*), triadin (*H* and *I*; and *T* and *U*), RyR1 (*J* and *L*; and *V* and *X*), and α1s-DHPR (*K* and *L*; and *W* and *X*). As reported, no differences in the organization of the sarcomeric and SR proteins between WT and sAnk1 KO are present (bar, 5 μm).

were applied in 10-mV steps from −70 to 50 mV. I_{Ca} was evaluated after subtracting linear capacitive and leak currents, using properly scaled control records. Control currents were obtained in response to 10-mV hyperpolarizing pulses from a holding potential of −100 mV.

Data Analysis

The time course of the macroscopic I_{Ca} was fitted by the sum of two-exponential functions as follows:

$$I_{Ca}(t) = I_{Ca,a}\exp\left[-(t - t_0)/\tau_a\right] - I_{Ca,i}\exp\left[-(t - t_0)/\tau_i\right] + C \quad (1)$$

where $I_{Ca}(t)$ is the current amplitude at time t after the depolarization; $I_{Ca,a}$ and $I_{Ca,i}$ are the amplitudes for each component representing the activation and inactivation time course, respectively; C is the steady state current; τ_a and τ_i are the time constants for the two components of the current time course; and t_0 is the tubular delay that, according to Ref. 14, was constrained to be 2 ms.

Equation 2, which follows below, was used to determine the voltage dependence of the $I_{Ca,a}$ curve:

$$I_{Ca,a}(V) = G_{max}(V - V_{rev})/\{1 + \exp[(V_a - V)/k_a]\} \quad (2)$$

where V_{rev} is the apparent reversal potential, G_{max} is the maximal conductance for the $I_{Ca,a}$ peak current, V_a is the voltage eliciting the half-maximal increase in conductance, and k_a is a steepness parameter.

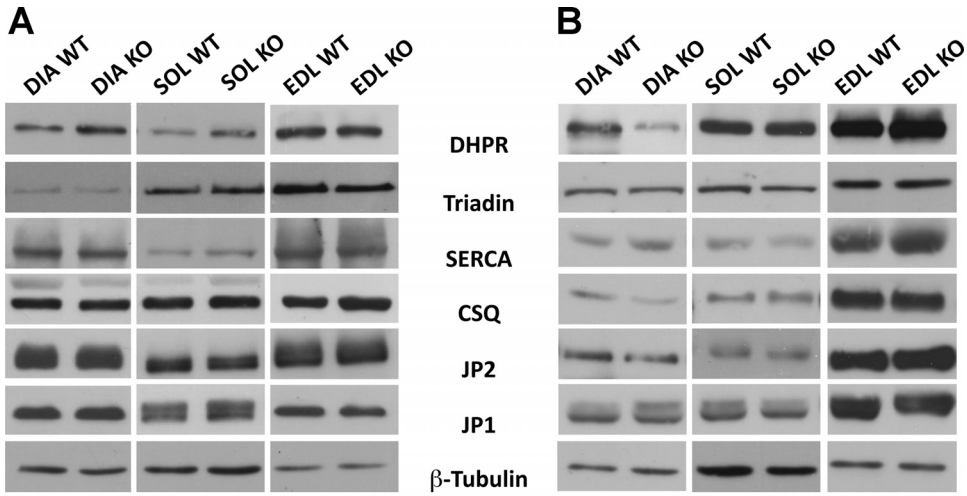

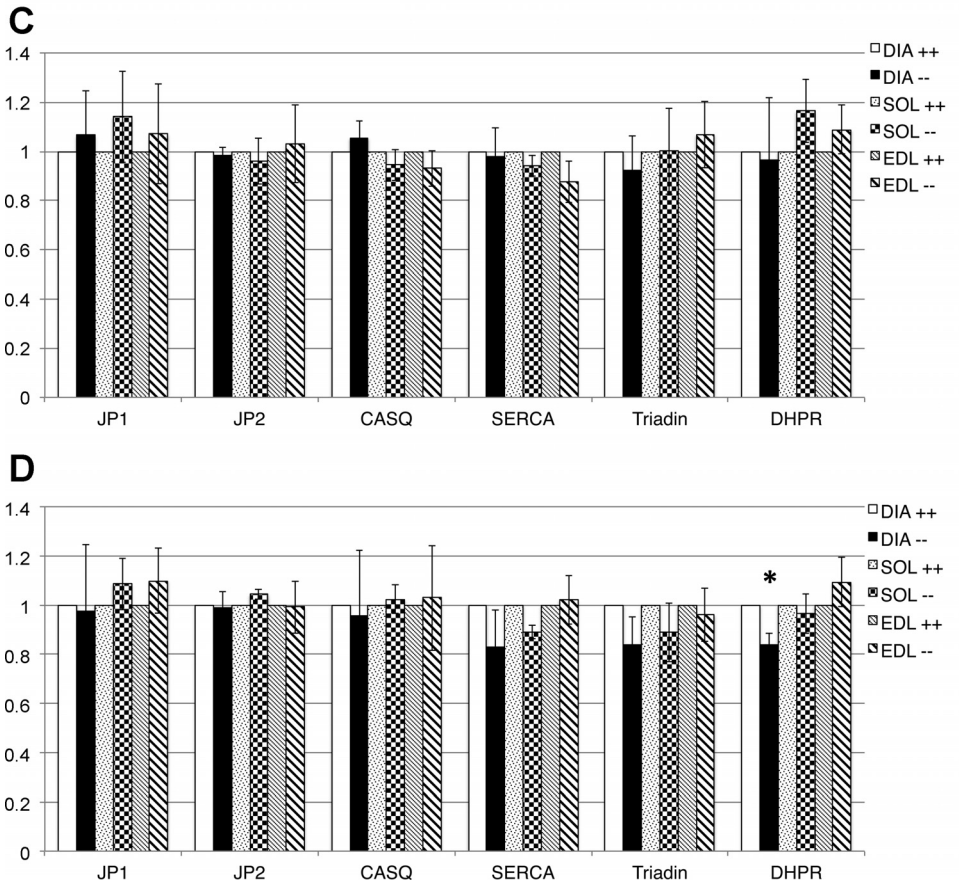

Fig. 3. SR protein expression levels in 4- to 6 mo-old sAnk1 KO mice, and 12- to 15-mo-old sAnk1 KO mice. Muscle extracts obtained from young (*A*) and old (*B*) sAnk1 KO and WT mice were subjected to SDS-polyacrylamide gel electrophoresis. Changes of protein expression levels were determined by Western blot analysis (*A* and *B*) and quantified by means of ImageJ software [young (*C*) and old (*D*)] as described in MATERIALS AND METHODS. *Statistically significant difference between WT and sAnk1 KO, with $P < 0.01$. DIA, diaphragm; SOL, soleus; JP1 and JP2, junctophillin-1 and -2.

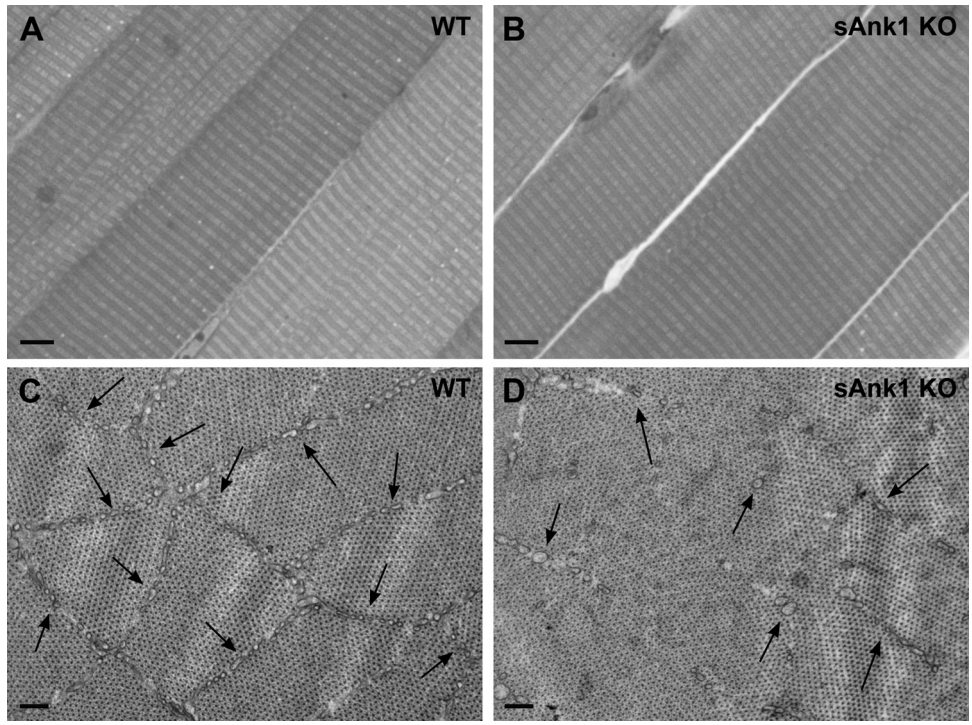

Fig. 4. A significant reduction in the SR at the A-band is observed in EDL fibers from adult sAnk1 KO mice. Histological examination of longitudinal sections did not reveal evident structural differences between WT (*A*) and sAnk1 KO (*B*) EDL muscles. EM analysis of cross sections at higher magnification revealed that longitudinal SR, visible as vesicles and tubules usually organized in a single layer between myofibrils (arrows), is reduced in fibers from sAnk1 KO mice (see Table 2 for quantitative analysis). Scale bars: *A* and *B*, 5 μm; *C* and *D*, 0.2 μm.

We considered $I_{Ca,a}(V)$ instead of the peak current $I_{Ca}(V)$, because significant inactivation can overlap the activation phase and consequently it could alter the apparent activation curve resulting directly from the peak value. I_{Ca} inactivation curves were evaluated using test pulses to 20 mV preceded by prepulses (1 s long, from −90 mV holding potential ranging from −80 to 50 mV, in 10-mV increments, interpulse intervals 200 ms). Inactivation curves were described using the Boltzmann function:

$$I(V) = 1/\{1 - \exp[(V - V_h)/k_h]\} \quad (3)$$

where V_h is the voltage at halfway between 1 and 0, and k_h is the constant that defines the voltage sensitivity. Currents were normalized to the linear capacitance measured by control pulses. The components of the ICM expressed in diaphragm muscle were evaluated following the previously described methods (6, 14, 35). Data fitting used a nonlinear curve fitting procedure based on the Marquardt-Levenberg algorithm (Sigmaplot 4 and Table Curve 3.10 by Jandel Scientific, and Clampfit 6.02 by Axon Instruments).

Statistical Analysis

Data are expressed as means ± SD, unless differently stated. Student's unpaired *t*-test was used for comparisons between sAnk1 KO and control data, and statistical significance was set at $P < 0.05$. GraphPad Prism software was used for curve fitting.

RESULTS

Generation of sAnk1 KO Mice

To study the role of the sAnk1 isoforms sAnk1 KO mice were generated. The mouse erythroid ankyrin gene, Ank1, contains 42 exons that code for the prototypical 210-kDa ankyrin protein, which is expressed primarily in red blood cells and the Purkinje cells of the cerebellum. In addition, the Ank1 gene encodes for a set of smaller (~20 kDa) Ank1 isoforms, sAnk1.5, 1.6, 1.7, and 1.9 (3, 8, 20, 21) that are expressed in skeletal muscle, through the use of an alternative promoter and first exon (exon 39a) located within intron 39 of the Ank1 gene (8). We used a gene targeting strategy to replace exon 39a with a neomycin-resistance cassette thereby creating a null mutation for all muscle-specific sAnk1s (Fig. 1*A*). Southern blot experiments (Fig. 1*B*) confirmed the insertion of the neomycin cassette, and Northern blot analysis (Fig. 1*C*) demonstrated the complete absence of all sAnk1 transcripts in sAnk1 KO hindlimb muscle RNAs. The targeted allele was made congenic on the C57BL/6J (B6) strain by backcrossing to the 10th

Table 1. *Morphometric analysis of the SR volume in WT and sAnk KO mice at 4–6 and 12–15 mo of age*

	A-Band SR Volume, %	
	WT	sAnk1 KO
EDL (5 mo old)	8.44 ± 1.48 (n = 51)	2.58 ± 0.67* (n = 49)
EDL (15 mo old)	8.53 ± 2.33 (n = 72)	2.36 ± 1.08* (n = 98)

Values are means ± SD. The A-band sarcoplasmic reticulum (SR) volume (expressed as relative fiber volume) in small ankyrin 1 knockout (sAnk1 KO) fibers is significantly reduced compared with wild-type (WT) at both 5 and 15 mo of age. EDL, extensor digitorum longus. *Statistically significant difference between WT and sAnk1 KO ($P < 0.05$).

Table 2. *Percentage of fibers containing TAs in old sAnk1 KO EDL*

	TAs, %	
	WT	sAnk1 KO
EDL (15 mo old)		57.5 ± 4.78* (n = 88)

Values are means ± SD. Fibers exhibiting tubular aggregates (TAs) were very frequent in EDL muscles of old sAnk1 KO mice, but absent in EDL muscles of age-matched WT mice. *Statistically significant difference between WT and sAnk1 KO ($P < 0.05$).

generation and then intercrossing to produce mice homozygous for the sAnk1 KO allele. Age-matched siblings homozygous for the wild-type sAnk1 allele were used as controls (WT). Two age groups of adult mice were used in this study, designated as young (4–6 mo) and old (12–15 mo). sAnk1 KO mice show normal viability, fertility, body weight, and life span.

Ablation of sAnk1 Does Not Alter the Localization and Expression of SR Proteins in Young Adult (4–6 mo) Mice, but Reduces the SR volume at the A Band

Immunostaining of skeletal muscle fibers of control WT mice with an antibody against sAnk1 isoforms resulted in the appearance of two bands, a prominent one at the level of the M-band and a less intense one at the level of the Z-disk (Fig. 2, *A* and *C*), in agreement with previously reported findings (3, 4, 22, 27). As expected, no sAnk1 signal was detected in longitudinal sections of sAnk1 KO mice muscles (Fig. 2, *M* and *O*). Identification of the Z-disk was obtained by staining skeletal muscle samples with an antibody against α-actinin (Fig. 2, *B, C, E*, and *F; N, O, Q*, and *R*). Immunostaining of skeletal muscle sections of control WT mice with an antibody against obscurin stained two bands, a stronger one at the level of the M-band and a dimmer one at the level of the Z-disk (Fig. 2, *D* and *F*). The abrogation of sAnk1 did not affect obscurin localization in sAnk1 KO mice (Fig. 2, *P* and *R*).

Given the reported evidence that sAnk1 plays a role in linking the SR to the sarcomere through specific binding to obscurin, we next investigated the localization of a selected group of SR and T-tubules proteins (RyR, SERCA1, triadin, and α1s-DHPR) in the EDL muscles of young sAnk1 KO mice. Immunostaining of sections of EDL muscle from sAnk1 KO and control muscles with antibodies against triadic proteins, i.e., triadin (Fig. 2, *H* and *I*; and *T* and *U*), RyR (Fig. 2, *J* and *L*; and *V* and *X*), and α1s-DHPR (Fig. 2, *K* and *L*; and *W* and *X*), resulted in a typical triadic pattern consisting of two bands flanking the Z disk region, in both sAnk1 KO and WT mice. The localization of the longitudinal SR protein SERCA1 was also not altered by sAnk1 deletion, as it was observed in a region of the SR in correspondence to the Z-disk region in skeletal muscle fibers from both sAnk1 KO and WT mice (Fig. 2, *G* and *I*, and *S* and *U*). Identical results were obtained in soleus, diaphragm, and tibialis anterior muscles (data not

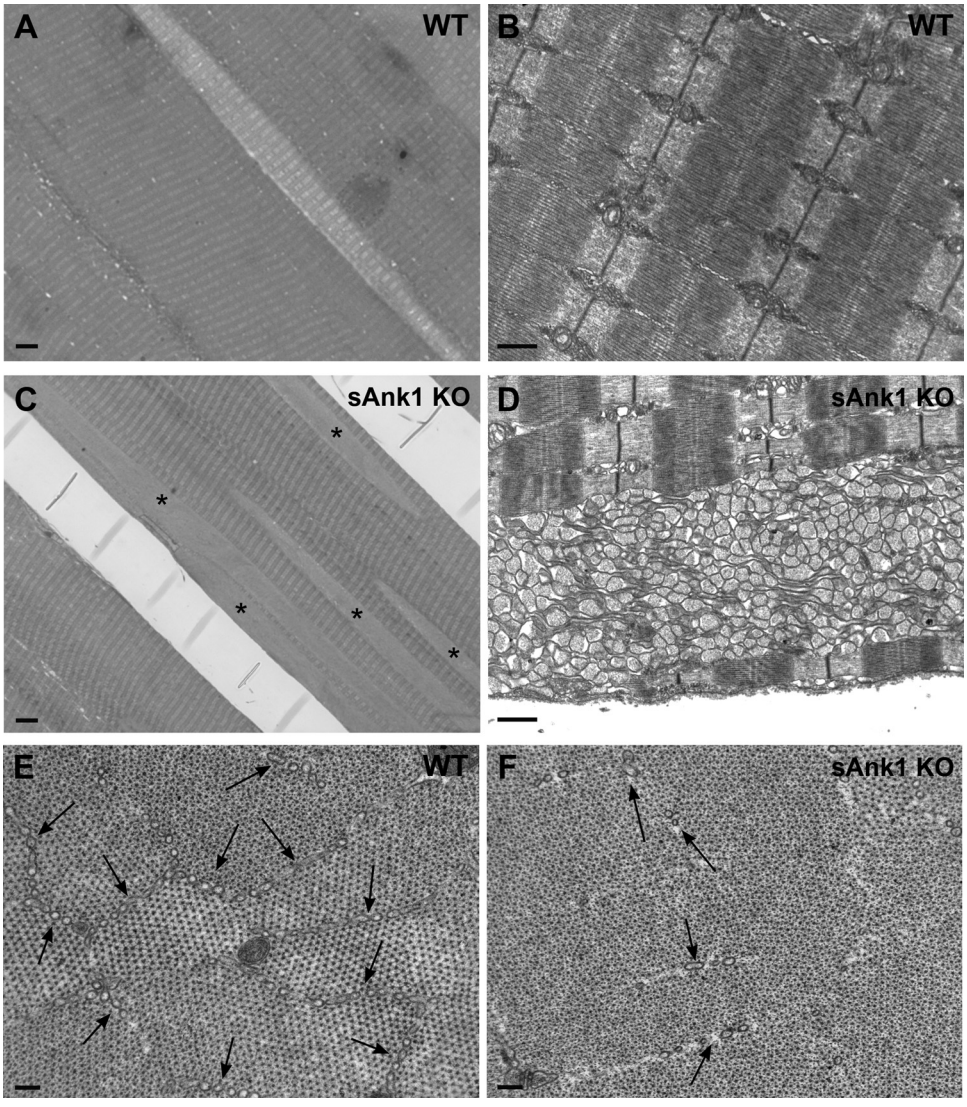

Fig. 5. EDL muscle of old sAnk1 KO mice show an age-dependent increase in the number of fibers containing TAs and a reduced SR volume compared with WT. EDL muscles of KO mice at 15 mo of age present high frequency of fibers presenting TAs (asterisks in *C* and enlargement in an EM micrograph in *D*) that are variable in size and are not (or very rarely) detected in age-matched WT mice (*A* and *B*; see Table 2 for quantitative analysis). A-band SR volume (arrows) is still significantly reduced in sAnk1 KO EDL fibers compared with WT (compare arrows in *E* and *F*), confirming data obtained in adult fibers (see Table 1 for quantitative analysis). Scale bars: *A* and *D*, 5 μm; *E* and *F*, 0.2 μm.

shown). The expression levels of some SR and T-tubule proteins were also analyzed by Western blot, but no significant differences in the expression levels of these proteins were observed between sAnk1 KO and WT young mice (Fig. 3, *A* and *C*).

The morphology of EDL skeletal muscle fibers from sAnk1 KO mice was also evaluated by histology and electron microscopy (EM). The overall sarcomeric architecture of adult sAnk1 KO mice skeletal muscle fibers was not apparently altered (Fig. 4*B*), as the regular cross striation typical of WT fibers was

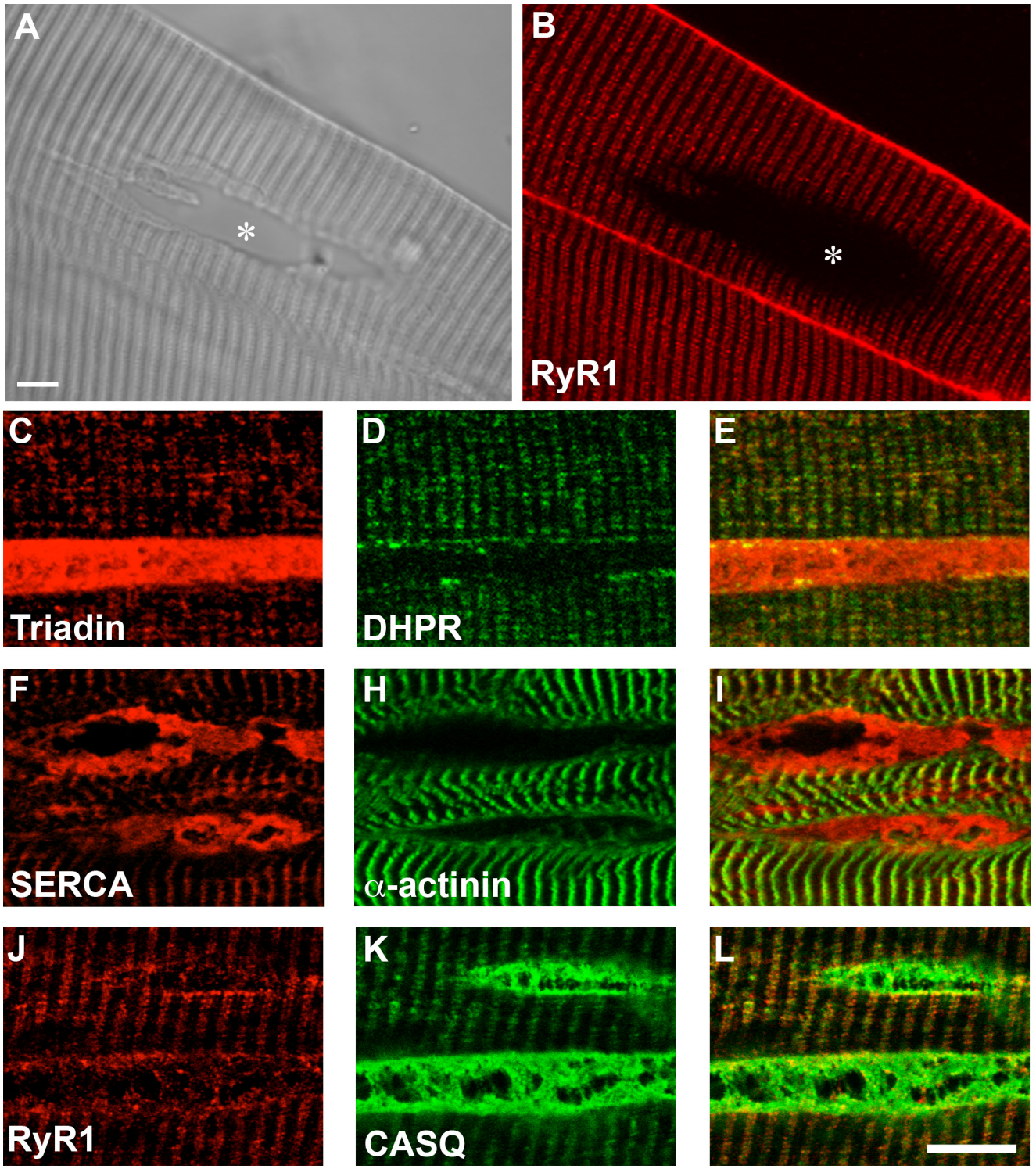

Fig. 6. TAs in old sAnk1 KO mice result positive for triadin, calsequestrin (CASQ), and SERCA1, but negative for RyR1 and α_1s-DHPR staining. In *A*, a phase-contrast image shows the position of a TA (asterisk). Immunostaining of 12- to 15-mo-old EDL fibers from sAnk1 KO mice with different antibodies specific for SR and T-tubules proteins reveals that TAs do not contain RyR1 (*B, J–L*) or α1s-DHPR (*D* and *E*) but are positive for triadin (*C* and *E*), calsequestrin (*K* and *L*), and SERCA1 (*F* and *I*). Scale bars: *A* and *B*, 5 μm; *C–L*, 10 μm.

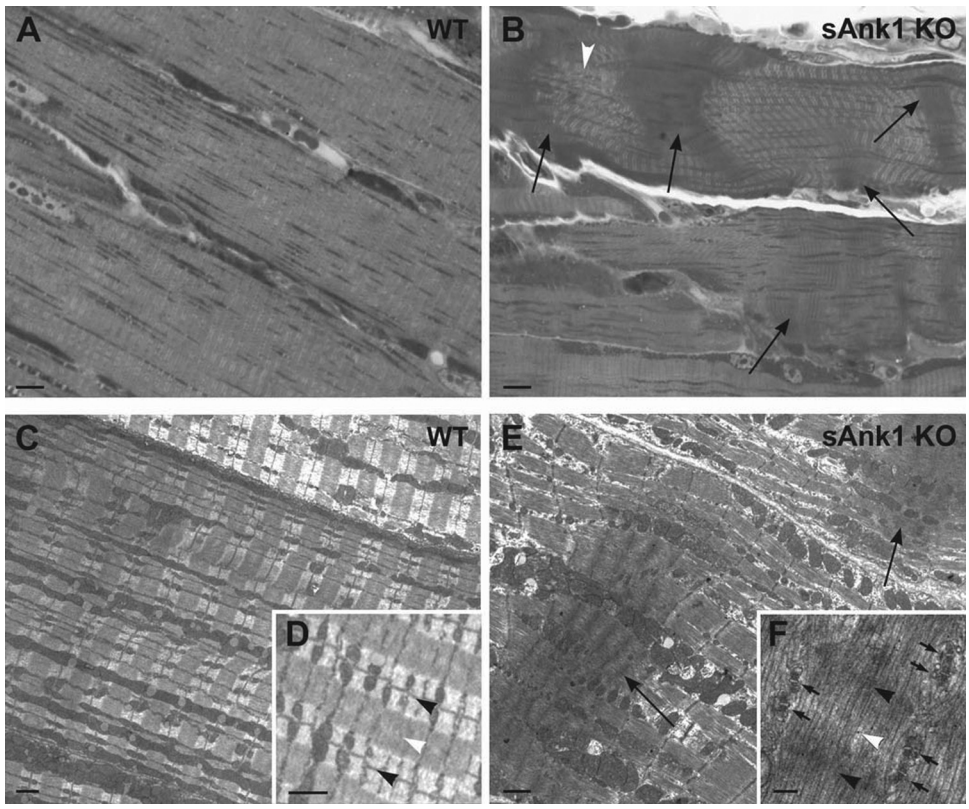

Fig. 7. Severe structural abnormalities in diaphragm muscle fibers from old sAnk1 KO mice revealed by light microscopy and EM. While diaphragm from WT mice maintains a well-preserved structure (*A* and *C*), sAnk1 KO fibers often exhibit large areas of contracture (arrows in *B* and *E*), just next to regions in which sarcomeres appeared normal or overstretched (*B*, white arrowhead). Within contracture regions, the regular disposition of intracellular organelles (such as triads, pointed by arrows in *F*) is abnormal with myofibrils that tend to fuse laterally. In *D* and *F* black arrowheads point at Z lines; white arrowhead points at the real (*D*) or putative (*F*) position of an M line. Scale bars: *A* and *B*, 5 μm; *C* and *E*, 1 μm; *D* and *F*, 0.2 μm.

quite well preserved (Fig. 4*A*). Z-disk and M-band of adjacent sarcomeres were well aligned with one another, with triads, correctly disposed and oriented at the A-I band transition (not shown). Also mitochondria were normally distributed on the two sides of the Z-lines and in close proximity to triads (not shown), as previously described (10). However, analysis of cross sections at higher magnification revealed that longitudinal SR, which at the A band level is visible as vesicles and tubules usually organized in a single layer between myofibrils (pointed by arrows in Fig. 4, *C* and *D*), was significantly reduced in fibers from sAnk1 KO mice. To support this visual observation we quantified the relative fiber volume occupied by the SR at the A band (expressed as a percentage of total fiber volume). This analysis confirmed the visual observation: A-band SR volume in EDL fibers was indeed significantly reduced in skeletal muscle fibers of sAnk1 KO mice compared with WT fibers: 2.58 ± 0.67% vs. 8.44 ± 1.48%, respectively (Table 1). Interestingly, these results closely mirror those reported in the characterization of obscurin KO mice by Lange et al. (28).

Structural Alterations Are Observed in EDL and Diaphragm Skeletal Muscle Fibers from Old Adult (12–15 mo) sAnk1 KO Mice

While morphological analysis of young sAnk1 KO mice did not reveal significant alterations other than the SR volume reduction, severe abnormalities were found in EDL and diaphragm muscles of older sAnk1 KO mice (12–15 mo). In EDL of this age the most frequent abnormality was the presence of large tubular aggregates (TAs) in a high percentage of fibers: 57.5 ± 4.78% (Table 2). These aggregates (Fig. 5, *C* and *D*) had variable size, and they were only rarely observed in age-matched controls (Fig. 5, *A* and *B*). TAs have been observed in a variety of congenital myopathies (i.e., neuromuscular disorders such as myotonic disorders, malignant hyperthermia, etc.), and also in skeletal muscle of inbred strains of mice, related to sex and age (2, 9, 11, 43). However, in WT muscle, TAs this frequent and of this size are usually found at later ages (9). To verify which SR and T-tubule proteins were present in these TAs, EDL fibers from old sAnk1 KO mice were immunolabeled with antibodies against RyR1 (Fig. 6, *B* and *J*), triadin (Fig. 6*C*), α1s-DHPR (Fig. 6, *D* and *E*), SERCA1 (Fig. 6, *F* and *I*), and calsequestrin (Fig. 6, *K* and *L*). TAs were positive for triadin, calsequestrin, and SERCA1 (Fig. 6, *C*, *F*, and K), but negative for α1s-DHPR and RyR1 (Fig. 6, *B*, *D*, and *J*). In parallel, as performed in young mice, expression levels of some SR and T-tubules proteins were also analyzed by Western blot in diaphragm, EDL, and soleus from old sAnk1 KO mice. No significant differences in the expression levels of analyzed proteins (triadin, SERCA1, calsequestrin, junctophillin 1 and 2, and α1s-DHPR) in EDL and soleus were observed. Interestingly, while the levels of other proteins analyzed did not change significantly, the levels of the α1s-DHPR protein were significantly reduced by ~15% in the diaphragm of old sAnk1 KO mice compared with age-matched WT mice (Fig. 3, *B* and *D*).

Furthermore, analysis of the relative volume occupied by the SR at the A-band (not including the regions containing TAs) in old sAnk1 KO mice confirmed the data obtained on KO mice at 4–6 mo of age, i.e., A-band SR was dramatically reduced (Table 1: 2.36 ± 1.08% vs. 8.53 ± 2.33% of WT; see also Fig. 5, *E* and *F*), suggesting that reduction of A-band SR volume did not progress significantly with time. It is important to

Table 3. *Percentage of fibers showing contractures in old sAnk1 KO diaphragm muscles*

	Contractures, %	
	WT	sAnk1 KO
Diaphragm (15 mo old)		61.5 ± 5.15 (n = 112)

Values are means ± SD. More than 60% of fibers in sAnk1 KO mice contain contractures at 12–15 mo of age.

mention that in a few EDL fibers some areas of excessive contracture and myofibrillar damage/degeneration were also found (data not shown).

Damage and degeneration, at this age (12–15 mo), was much more severe in the diaphragm. Indeed, histological and EM analysis of the diaphragm muscle of KO mice revealed the presence of large areas of contracture in many fibers (black arrows in Fig. 7, *B* and *E*), alternated with regions in which the length of sarcomeres was overstretched or apparently normal (white arrowhead in Fig. 7*B*). Contractures were observed in 61.5 ± 5.15% of diaphragm muscle fibers from 12- to 15-mo-old sAnk1 KO mice (Table 3), whereas they were never found in aged-matched control mice (Fig. 7, *A* and *C*). In contractured regions intermyofibrillar organelles, such as mitochondria or triads, were misplaced or missing (arrows in Fig. 7*E*) with contracted myofibrils, which appear fused laterally with each other.

Altered Contractile Function Is Observed in sAnk1 KO Skeletal Muscles

To verify the impact of sAnk1 deletion on skeletal muscle performance, we investigated the contractile properties of EDL, soleus, and diaphragm muscles dissected from sAnk1 KO and control mice of 4–6 and 12–15 mo of age. Time to peak, half-relaxation time, twitch tension, and tetanus tension were measured. No significant difference was found in EDL and soleus muscles from sAnk1 KO and control mice of 4–6 mo of age (Fig. 8). In contrast, in diaphragm muscle of 4- to 6-mo-old sAnk1 KO mice, time to peak was prolonged compared with age-matched control mice. Additional differences were observed when the analysis was performed on skeletal muscles from sAnk1 KO mice of 12–15 mo of age (Fig. 8). In the EDL muscle of these mice, time to peak and half-relaxation time were longer in sAnk1 KO mice than in control mice, while twitch tension and tetanus tension showed no significant difference. In the diaphragm from 12- to 15-mo-old sAnk1 KO mice, time to peak tension and half-relaxation time were prolonged, and twitch and tetanic tension were reduced (Fig. 8). No difference was observed in soleus muscle from mice of 12–15 mo of age compared with age-matched controls.

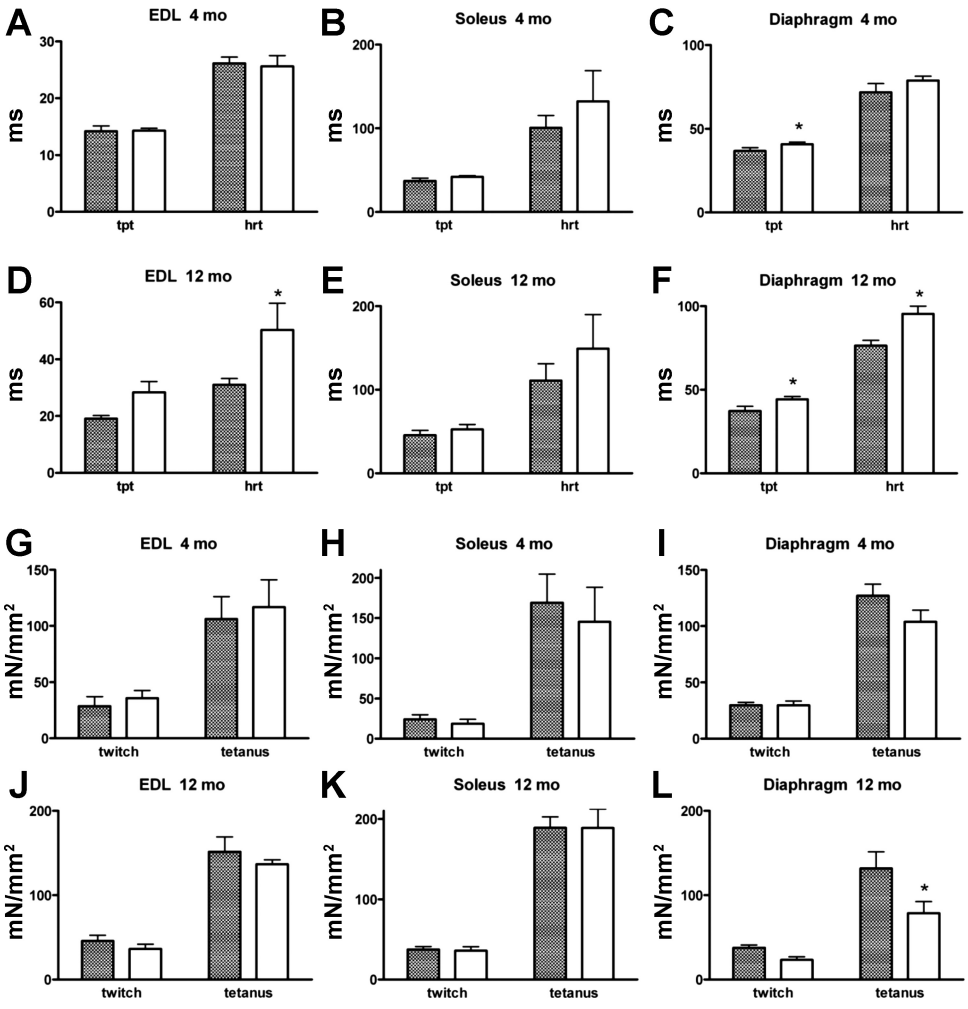

Fig. 8. Time and force parameters of the contractile response of muscles from WT and sAnk1 KO mice. Time and force parameters of the contractile response of EDL, soleus, and diaphragm muscles from adult (4–6 mo) and old (12–15 mo) WT (filled columns) and sAnk1 KO (white columns) mice. Time parameters [time to peak tension (tpt) and half-relaxation time (hrt)] expressed in ms are shown in histograms in *A–F*. Peak tension generated during isometric twitch and tetanus are shown in histograms in *G–L*. Means ± SE. *Statistically significant difference between WT and sAnk1 KO ($P < 0.05$).

To further evaluate the impact of sAnk1 ablation on skeletal muscle contractile function in vivo, additional experiments were performed only with sAnk1 KO mice of 12–15 mo of age. Isometric contraction of gastrocnemius was induced in vivo via nerve stimulation at various frequencies. Twitch, partially fused tetanus, and complete fused tetanus revealed no significant difference in torque development between sAnk1 KO and WT mice (data not shown). In contrast, twitch kinetics were slower in sAnk1 KO as indicated by the significant prolongation of twitch time to peak, as shown in Fig. 9*A*. Muscle strength in voluntary contractions was also tested in in vivo experiments on 12- to 15-mo-old sAnk1 KO mice. According to the grip test protocol, which evaluates the instinctive grasp force of both anterior and posterior limbs, 12- to 15-mo-old sAnk1 KO performed similarly to control mice (Fig. 9*B*). In contrast, when the endurance of sAnk1 KO mice was analyzed in a treadmill test, where animals were left running until exhaustion, sAnk1 KO mice showed a significantly reduced performance, as these mice were able to run only for half the time or distance covered by age-matched control mice (Fig. 9*C*).

Altered Sarcolemmal Electrophysiological Features in sAnk1 KO Skeletal Muscles

The first step in e-c coupling is a voltage-sensing process consisting of the change of charged particles orientation within the dihydropyridine receptors located in the T tubules. This is detected as intramembrane charge movement (ICM) and it shows at least two components (Q_β and Q_γ) in normally polarized skeletal muscle fibers of the frog (31, 37, 44) and mammals (6, 14, 35). Dihydropyridine receptors are voltage sensors for RyR opening and functional L-type Ca^{2+} channels (L-CaC). Q_γ charge is related to L-CaC and RyR opening since its occurrence is followed by L-type Ca^{2+} current (I_{Ca}) and Ca^{2+} release from SR. Thus their eventual modifications may be considered as an index of an e-c coupling alteration (14, 6, 35). Therefore, we sought to verify whether the morphological and contractile alterations of the skeletal muscle fibers of KO animals were accompanied by modifications of the electrophysiological properties of the sarcolemma and of the e-c coupling. To this end, we focused on the Q_γ charge component of ICM and I_{Ca} in EDL and diaphragm (DIA) muscles.

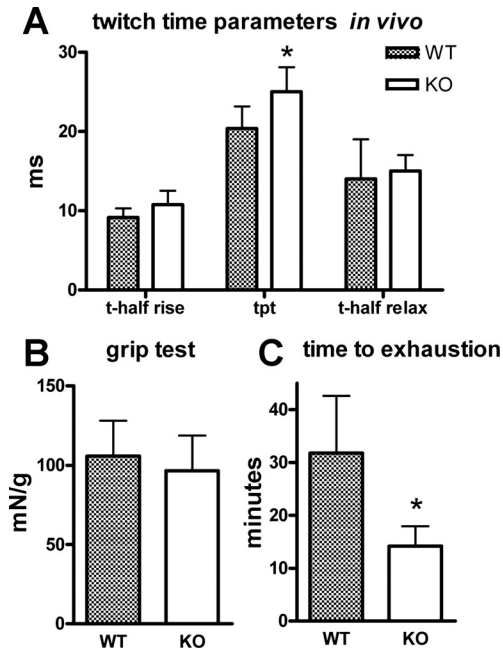

Fig. 9. Analysis of muscle contractile performance in vivo reveals differences between sAnk1 KO and WT old mice. Twitch kinetics measured in vivo by gastrocnemius stimulation via nerve were slower in 12- to 15-mo-old sAnk1 KO compared with WT mice, as indicated by the significant prolongation of twitch time to peak in *A*. In *B*, grip test results are reported: WT and sAnk1 KO mice generated similar force at limb level; whereas, as shown in *C*, sAnk1 KO mice showed a drastic reduction of the performance in exhaustion time in a treadmill endurance test. Values are shown as means ± SD. *Significantly different at $P < 0.05$.

Muscles obtained either from sAnk1 KO or control mice displayed significant differences with age in the resting membrane potential (RMP), membrane capacitance (C_m), specific resting membrane conductance (G_m/C_m), and L-type Ca^{2+} current density (I_{Ca}/C_m) (Fig. 10, *A–D*). Interestingly, only fibers from the diaphragm of 12- to 15-mo-old sAnk1 KO mice showed significant differences in all the above parameters compared with age-matched control mice. Indeed, as shown in Fig. 10, the RMP recorded in diaphragm fibers was ~11 mV less negative in 12- to 15-mo-old sAnk1 KO with respect to age-matched WT (Fig. 10*A*), and this was paralleled by reduced values of C_m (Fig. 10*B*), G_m/C_m (Fig. 10*C*), and I_{Ca}/C_m, (Fig. 10*D*). All these data respectively suggest a condition of fiber atrophy, an increased leak current, and an affected e-c coupling. Here, we report in detail only the results on ICM and I_{Ca} obtained in diaphragm fibers from WT and sAnk1 KO old mice. Figure 11 shows a family of current records obtained from a diaphragm fiber from a WT (Fig. 11*A*) and a sAnk1 KO (Fig. 11*B*) old mouse. The transient outward nonlinear current at the beginning of each trace was primarily due to ICM. Above −30 mV ICM was followed by a more slowly appearing inward current. Since this was completely blocked by nifedipine we assumed it was I_{Ca}. To evaluate clearly ICM time course we had to minimize the overlapping I_{Ca}. To this end we made a multiexponential fit to I_{Ca} time course and then we subtracted the fit from the related total current traces (see 6, 15). Simple visual comparison of the representative ICM currents in Fig. 11, *C–K*, reveals several similarities and differences between charge movement currents recorded from the WT and sAnk1 KO fibers. For depolarizing steps from −70 to −40 mV, where only Q_β charge is moved, the amplitude of the transient currents and their time course were similar for WT and KO fibers.

For voltage pulses from −30 mV, the charge movement records from the WT fibers exhibited a temporally delayed "hump" component after the initial peak suggesting the occurrence of Q_γ charge, whereas sAnk1 KO fibers continued to display an ICM time course consisting of a relatively rapid rise followed by a monotonic decay, that was likely Q_β. To evaluate the entity of the different charge moved in WT and sAnk1 KO we subtracted the sAnk1 KO from the corresponding WT current. The result was a null current from −70 to −40 mV (green traces in Fig. 11, *C–K*) and transient traces above these voltages, indicating a decreased Q_γ charge in sAnk1 KO. To test further such outcomes, we evaluated the total charge moved, Q_{ICM}, as a function of voltage (Q_{ICM}–*V* plot). In WT fibers, the $Q_{ICM,on}$–*V* plots (Fig. 10*E*) showed a complex form because of the presence of two different slopes; accordingly,

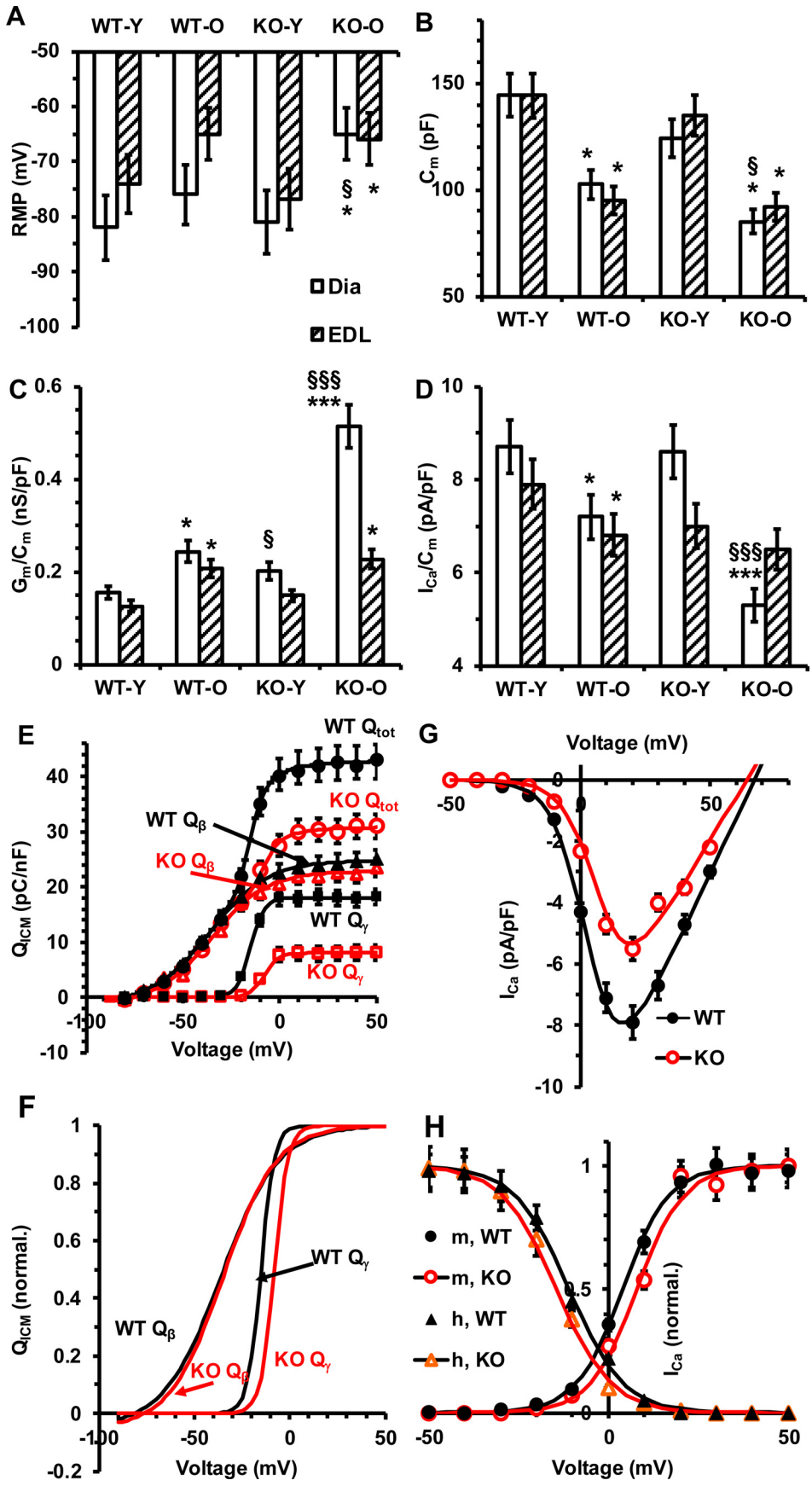

Fig. 10. Diaphragm fibers from old sAnk1 KO mice display altered electrophysiological parameters. Resting membrane potential (RMP; *A*), membrane capacitance (C_m; *B*), specific resting membrane conductance (G_m/C_m; *C*), and L-type Ca^{2+} current density (I_{Ca}/C_m; *D*) in diaphragm (Dia) and EDL fibers from young (Y) and old (O) control and sAnk1 KO mice. $*P < 0.05$, $***P < 0.001$, old compared with corresponding young fibers; §$P < 0.05$, §§§$P < 0.001$, sAnk1 KO compared with related WT fibers. Only data from old sAnk1 KO diaphragms were statistically different from old WT diaphragms. WT-Y, WT-O, KO-Y, and KO-O indicate WT young, WT old, KO young, and KO old mice, respectively. *E*: Q_{ICM}–*V* relationship of total charge moved (Q_{tot}) and fits related to the single components Q_β and Q_γ. Steady-state voltage distribution of the amount of charge moved, Q_{tot}, in WT (filled symbols) and KO fibers (open symbols) from old diaphragms. The continuous line through $Q_{ICM,tot}$ data is the best fit as a sum of two Boltzmann terms. ICM, intramembrane charge movement. *F*: normalized Q_β and Q_γ charge. The lines indicated as Q_β and Q_γ are the calculated curves related to each single Boltzmann term, for WT (black) and sAnk1 KO DIA (red). *G*: I_{Ca}–*V* plot of WT (black) and sAnk1 KO (red). *H*: normalized I_{Ca} activation (m) and inactivation (h) plots. Data are means ± SE from 9 WT-Y, 8 WT-O, 8 KO-Y, and 8 KO-O mice and, respectively, 22, 23, 21, and 20 EDL, and 18, 20, 19, and 22 DIA fibers.

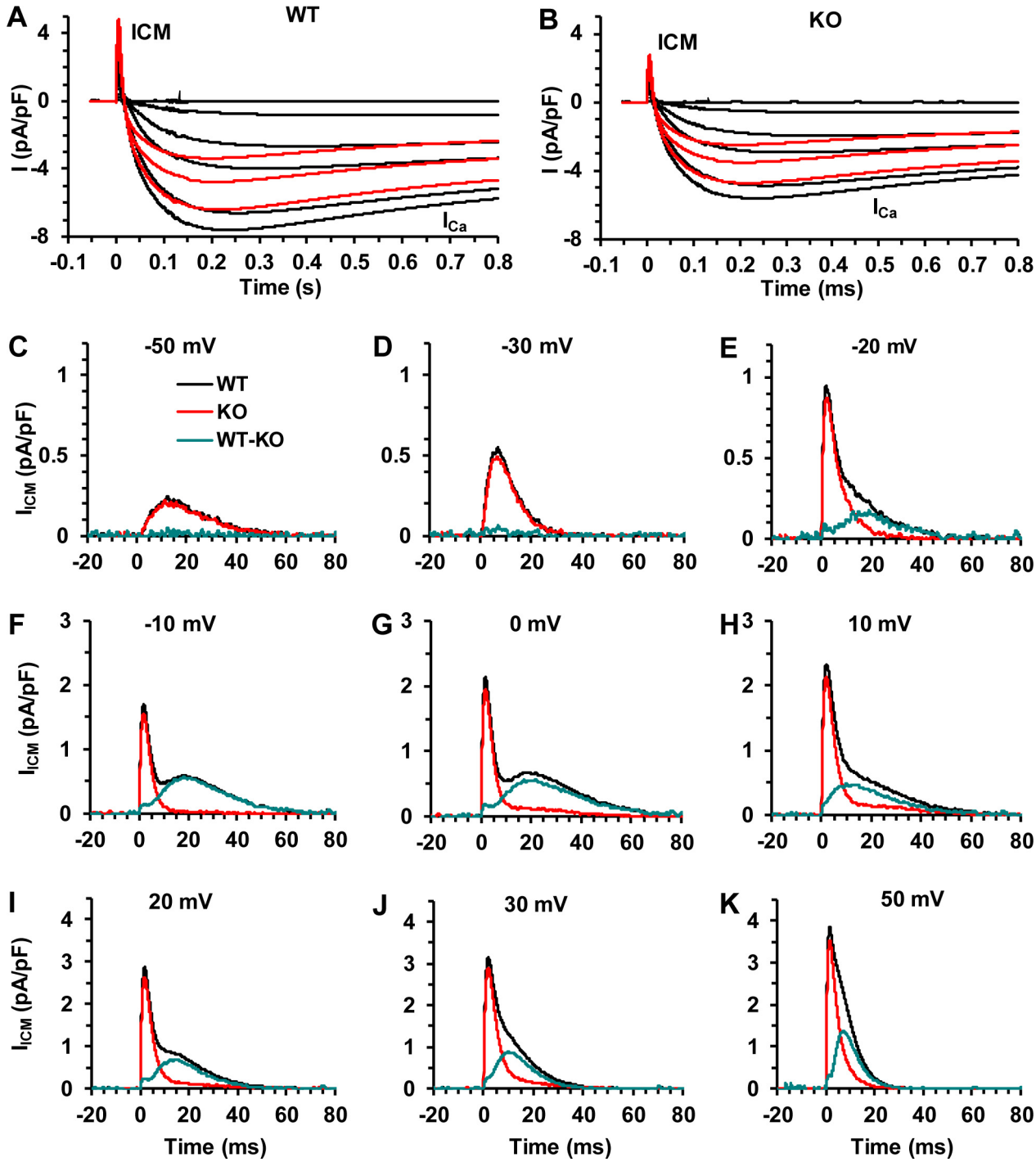

Fig. 11. ICM and L-type Ca^{2+} currents (I_{Ca}) in sAnk1 KO old diaphragms fibers are depressed compared with WT. *A* and *B*: typical families of current traces showing an early outward current, IICM, followed by inward I_{Ca} in WT (*A*) and KO fibers (*B*); traces elicited by voltage steps from −70 to 20 mV are depicted in black and those from 30 to 50 mV are in red. *C–K*: typical IICM in WT (black), KO (red), and differences WT-KO (green) evoked by the voltage step indicated in each panel. Note the different ordinate scale in *C–E*, with respect to *F–H* and *I–K* panels. Note the reduction of the temporally delayed "hump" Qγ component in KO fibers (*E–G*).

the best fit was achieved by a two Boltzmann-term function. In contrast, the plot of sAnk1 KO perfectly superimposed to WT up to −40 mV, but for more depolarized potentials it was different since it showed a reduced second term. By comparing the single Boltzmann terms of the plots we did not observe any statistical difference in Q_β charge, whereas Q_γ was the only component depressed in sAnk1 KO fiber mice (Table 4). Moreover, Q_γ activation was positively shifted ~10 mV (Fig. 10*F*, Table 4). The Q_γ changes were paralleled by an analogous decrease of I_{Ca}/C_m value, estimated at the current peak (Fig. 10*G*). Such a decrease in sAnk1 KO fibers suggests a reduced number of functional L-type Ca^{2+} channels. These

Table 4. *Boltzmann parameters of Q_β and Q_γ mobilization in WT and KO fibers of diaphragm muscles from old mice*

Parameters	WT	KO
$Q_{\beta max}$, pC/nF	26.2 ± 3.0	24.1 ± 2.5
V_β, mV	−36 ± 3.2	−35 ± 3.6
k_β, mV	15 ± 1.3	14 ± 1.4
$Q_{\gamma max}$, pC/nF	18 ± 1.5	8.1 ± 0.7*
V_γ, mV	−15 ± 1.2	−8.1 ± 1.3*
k_γ, mV	3.5 ± 0.4	3.6 ± 0.4

Data are means ± SE from 20 (8 WT mice) and 22 (8 KO mice) diaphragm fibers. sAnk1 KO mice show a significant decrease of the steady-state amount of the Q_γ charge moved, $Q_{\gamma max}$, and a shift towards more positive potential of V_γ but not of Q_β parameters. *$P < 0.01$, KO parameters with respect to WT.

data are in agreement with the observed decrease of α1s-DHPR protein detected by Western blot analysis of old sAnk1 KO diaphragms.

The changes of the Boltzmann parameters pointed out a progressive alteration of I_{Ca} activation and inactivation kinetics (Table 5). In fact, V_a was positively shifted 2.3 mV and V_i was negatively shifted ~4.8 mV in sAnk1 KO with respect to control wild-type mice (Fig. 10*H*). Finally, V_{rev} was negatively shifted ~6.3 mV (Fig. 10*G*, Table 5).

Together with the increased G_m/C_m value, this could suggest an increased intracellular Ca^{2+} concentration, likely due to a leakiness in the sarcolemma. To verify this possibility we performed the Evans blue dye test in old mice, which is regularly used to test sarcolemma integrity (46). Interestingly, we observed a significant increase in the percentage of Evans blue positive fibers in old sAnk1 KO mice compared with WT mice (3.20 ± 1.62 and 0.88 ± 1.12, respectively; $P < 0.009$).

DISCUSSION

A remarkable level of organization of the SR is observed in striated muscle cells. Longitudinal and junctional SR regions are regularly aligned with respect to specific regions of the sarcomere, with an outstanding alternating pattern that encircles the myofibrils. The organization of the SR with respect to the sarcomere is regarded as essential for the regulation of muscle contraction (16, 38, 45). To further increase our knowledge on the relevance of sAnk1 in the maintenance of this organized connection between the SR and the myofibrils, we generated KO mice selectively lacking sAnk1 isoform expression. The analysis of striated muscles from KO mice revealed that the main effect of sAnk1 ablation in skeletal muscle is the reduction of the longitudinal SR at the A band, which is in agreement with the preferential localization of sAnk1 in the longitudinal SR at the M band level. This last observation is reminiscent of previous results obtained in studies of skeletal muscles from obscurin KO mice, reporting an altered distribution of the longitudinal SR over the contractile cytoskeleton (28). Morphological alterations of the SR, mainly at the level of longitudinal SR organization, with only minimal involvement of the junctional SR, have also been obtained using a knockdown approach in adult skeletal muscle fibers (1). At the functional level, though, the reduction in SR volume observed in sAnk1 KO mice of 4 mo was accompanied by prolonged twitch time parameters only in the diaphragm muscle, but not in EDL and soleus muscles. This may be explained by the preserved content of SERCA1.

The availability of sAnk1 KO mice allowed us to follow the effect of sAnk1 ablation also at more advanced ages. If functional changes at 4 mo of age are not very evident in most muscles, with increasing age, KO mice develop a myopathy characterized by severe structural alterations: premature formation of large TAs in EDL, accompanied by structural damage of contractile elements, which is very severe especially in the diaphragm (interestingly the muscle that functionally was already more affected at 4 mo).

TAs have been observed in skeletal muscle of humans and mice, where they are related to sex and age and have been proposed to rise from misfolding and aggregation of membrane proteins due to altered proteostasis (43). Interestingly, they have been reported to be associated with congenital myopathies (2, 11). Formation of large areas of contracture and degeneration of contractile elements have been described also in other animal models of muscle diseases characterized by intracellular imbalance of Ca^{2+} levels. Not surprisingly, such severe alterations were accompanied by significant functional impairment (slower twitch kinetics), which at 12 mo of age are also evident in fast hindlimb muscles (EDL ex vivo and gastrocnemius in vivo). In addition, diaphragm contraction showed a significant reduction in the ability to develop force, which can be attributed to the loss of functioning fibers. The reduction in the in vitro performance of skeletal muscles of 12-mo-old sAnk1 KO mice was mirrored by their dramatically reduced endurance in treadmill tests. Worthy of further investigation is the fact that soleus muscle was not significantly affected by the ablation of sAnk1.

How to reconcile the reduced volume of the SR observed in sAnk1 KO mice with the alterations observed in selected muscle and their worsening with age is not obvious, but certainly the effects of sAnk1 deletion are stronger in the diaphragm muscle at 12 mo of age. This was further reinforced by electrophysiological experiments, performed in old sAnk1 KO mice, that together with the Evans blue dye test, revealed altered properties of the sarcolemmal membrane, such as a depolarized RMP and an increased specific membrane conductance, G_m/C_m, paralleled by a reduced Q_γ charge and I_{Ca}/C_m. Such observations suggest that *1*) sarcolemma integrity was lost with a possible alteration of cytosolic Ca^{2+} concentration which, in the long run, might lead to contractures and marked structural alterations; and *2*) e-c coupling was altered and this might contribute to the significant increase in the half-relaxation time and the decrease of the tetanic force. In summary, the reduction of Q_γ and I_{Ca} size and tetanic contractions

Table 5. *Boltzmann parameters of I_{Ca} activation and inactivation in diaphragm fibers from WT and KO old mice*

Parameters	WT	KO
G_m, nS/pF	181.2 ± 15	139.5 ± 12*
V_a, mV	3.9 ± 0.3	6.2 ± 0.4*
k_a, mV	6.4 ± 0.3	7.1 ± 0.4*
V_{rev}, mV	69.4 ± 5	63.1 ± 4*
V_h, mV	−10.9 ± 1.2	−14.7 ± 1.3*
k_h, mV	7.5 ± 0.4	7.6 ± 0.4

Data are means ± SE. Data are from the same fibers reported in Table 4. I_{Ca}, L-type Ca^{2+} current. sAnk1 KO mice show a significant decrease of all the steady-state Boltzmann activation and inactivation parameters of I_{Ca} except for k_h. *$P < 0.05$, KO parameters with respect to WT. See *Data Analysis* for further description of parameters.

observed prevalently in old diaphragm muscle could denote that sAnk1 acts, even if indirectly, as a positive regulator of e-c coupling and in turn with force generation mostly in ageing. Prolongation of time to peak and half-relaxation time can be explained by an impaired Ca^{2+} reuptake in turn related to the partial loss of longitudinal SR, where SERCA pumps are localized, even though SERCA1 levels were not affected. It can be hypothesized that the loss of SR volume in young animals is somehow counterbalanced by other compensative mechanisms. In fact, the effects of the loss of SR volume become more evident with age and particularly in the diaphragm muscle, probably because of the continuous activity of this muscle. This, with time, may elicit complications that could not be further compensated, as it may occur in less intensely used muscles. These alterations would ultimately lead to altered membrane permeability and contribute to the observed muscle dysfunction. The lack of an impact of sAnk1 ablation on soleus muscle may be explained by the peculiar features of calcium homeostasis in slow fibers. Actually, in slow fibers, at variance with fast fibers, a much lower amount of calcium is released by each action potential in relation to specific binding properties of troponin C and to the absence of parvalbumin (5). Moreover, the density of the calcium pump SERCA1 is proportionally lower compared with fast fibers (33, 48).

Although, also due to the different approach (knockdown by siRNA vs. gene KO), it is not possible to directly compare our results with the functional relevance of the effect of knockdown of sAnk1.5 in muscle fibers obtained by Ackermann et al. (1), it is worth noting that the overall phenotype of sAnk1 KO muscle reported here is more severe than that described in skeletal muscles of obscurin KO mice by Lange et al. (28). Indeed, the obscurin KO mice presented lower levels of sAnk1.5 protein associated with a reduced amount of SR around the A band of sarcomeres in the myofibrils. In addition, by 1 yr of age, they developed an increased number of centrally localized nuclei, which suggests a mild form of myopathy. However, neither additional structural alterations in the SR or in the contractile apparatus, nor alterations in skeletal muscle contractile properties were observed in obscurin KO mice. The relatively milder effects of obscurin deletion compared with sAnk1 deletion is somehow surprising if one considers that obscurin and sAnk1 proteins are supposed to directly interact with each other in order to connect and stabilize the SR around the myofibrils. Other mechanisms could explain the more severe phenotype. In this context, it is worth noting that sAnk1.5 has been also found to participate in a multiprotein complex with Tmod3 and other proteins like γ-cyto-actin, Tm4, and Tm5NM1 (24). In skeletal muscles lacking tropomodulin 1, the interaction between sAnk1 and Tmod3 and other proteins was lost with sAnk1.5 being mislocalized at the Z-line. This was accompanied by changes in the SR morphology with swelling phenomena, by a defective Ca^{2+} release and by an age-dependent increase of sarcomere misalignment. These results differ from those obtained in obscurin KO mice that display SR retraction from the M-band, but showed no alteration in muscle contraction. To determine whether the different effects observed in the three independent mice models (lacking obscurin, sAnk1, or Tmod1, respectively, in skeletal muscles) reflect distinct, but complementary, roles of the obscurin-sAnk1.5 and Tmod3-sAnk1.5 complexes in the organization of SR membranes around the myofibrils and/or additional specific roles sustained by these proteins will require further experimental analysis.

GRANTS

This work was supported by Telethon Grant GGP13213 to V. Sorrentino, F. Protasi, and C. Reggiani; by MIUR PRIN 2009 Grant 2009YHXJ85 to V. Sorrentino and C. Paolini; and by Regione Toscana Grant "Bando Salute 2009" 132 to E. Giacomello.

Present address for M. Quarta: Dept. of Neurology and Neurological Sciences and Paul F. Glenn Laboratories for the Biology of Aging, Stanford Univ., Stanford, CA 94305.

DISCLOSURES

No conflicts of interest, financial or otherwise, are declared by the author(s).

AUTHOR CONTRIBUTIONS

Author contributions: E.G., M.Q., C.B., L.P., F.F., C.R., and V.S. conception and design of research; E.G., M.Q., C.P., R.S., P.F., L.T., B.B., L.F., D.R., C.B., F.F., and C.R. performed experiments; E.G., M.Q., C.P., B.B., C.R., and V.S. interpreted results of experiments; E.G., M.Q., C.P., R.S., P.F., L.T., B.B., C.B., F.F., and C.R. prepared figures; E.G., M.Q., C.P., and V.S. drafted manuscript; E.G., M.Q., C.P., R.S., P.F., L.T., B.B., L.F., D.R., C.B., L.P., F.F., F.P., C.R., and V.S. approved final version of manuscript; E.G., M.Q., C.P., R.S., P.F., L.T., B.B., L.P., F.F., F.P., C.R., and V.S. analyzed data; E.G., C.P., R.S., C.B., F.F., C.R., and V.S. edited and revised manuscript.

REFERENCES

1. **Ackermann MA, Ziman AP, Strong J, Zhang Y, Hartford AK, Ward CW, Randall WR, Kontrogianni-Konstantopoulos A, Bloch RJ.** Integrity of the network sarcoplasmic reticulum in skeletal muscle requires small ankyrin 1. *J Cell Sci* 124: 3619–3630, 2011.
2. **Agbulut O, Destombes J, Thiesson D, Butler-Browne G.** Age-related appearance of tubular aggregates in the skeletal muscle of almost all male inbred mice. *Histochem Cell Biol* 114: 477–481, 2000.
3. **Armani A, Galli S, Giacomello E, Bagnato P, Barone V, Rossi D, Sorrentino V.** Molecular interactions with obscurin are involved in the localization of muscle-specific small ankyrin1 isoforms to subcompartments of the sarcoplasmic reticulum. *Exp Cell Res* 312: 3546–3558, 2006.
4. **Bagnato P, Barone V, Giacomello E, Rossi D, Sorrentino V.** Binding of an ankyrin-1 isoform to obscurin suggests a molecular link between the sarcoplasmic reticulum and myofibrils in striated muscles. *J Cell Biol* 160: 245–253, 2003.
5. **Baylor SM, Hollingworth S.** Sarcoplasmic reticulum calcium release compared in slow-twitch and fast-twitch fibres of mouse muscle. *J Physiol* 551: 125–138, 2003.
6. **Bencini C, Squecco R, Piperio C, Formigli L, Meacci E, Nosi D, Tiribilli B, Vassalli M, Quercioli F, Bruni P, Zecchi Orlandini S, Francini F.** Effects of sphingosine 1-phosphate on excitation-contraction coupling in mammalian skeletal muscle. *J Muscle Res Cell Motil* 24: 539–554, 2003.
7. **Bennett V, Baines AJ.** Spectrin and ankyrin-based pathways: metazoan inventions for integrating cells into tissues. *Physiol Rev* 81: 1353–1392, 2001.
8. **Birkenmeier CS, Sharp JJ, Gifford EJ, Deveau SA, Barker JE.** An alternative first exon in the distal end of the erythroid ankyrin gene leads to production of a small isoform containing an NH2-terminal membrane anchor. *Genomics* 50: 79–88, 1998.
9. **Boncompagni S, Protasi F, Franzini-Armstrong C.** Sequential stages in the age-dependent gradual formation and accumulation of tubular aggregates in fast twitch muscle fibers: SERCA and calsequestrin involvement. *Age* 34: 27–41, 2012.
10. **Boncompagni S, Rossi AE, Micaroni M, Beznoussenko GV, Polishchuk RS, Dirksen RT, Protasi F.** Mitochondria are linked to calcium stores in striated muscle by developmentally regulated tethering structures. *Mol Biol Cell* 20: 1058–1067, 2009.
11. **Chevessier F, Marty I, Paturneau-Jouas M, Hantai D, Verdiere-Sahuque M.** Tubular aggregates are from whole sarcoplasmic reticulum origin: alterations in calcium binding protein expression in mouse skeletal muscle during aging. *Neuromuscul Disord* 14: 208–216, 2004.

12. **Connolly AM, Keeling RM, Mehta S, Pestronk A, Sanes JR.** Three mouse models of muscular dystrophy: the natural history of strength and fatigue in dystrophin-, dystrophin/utrophin-, and laminin alpha2-deficient mice. *Neuromuscul Disord* 11: 703–712, 2001.
13. **Cunha SR, Mohler PJ.** Obscurin targets ankyrin-B and protein phosphatase 2A to the cardiac M-line. *J Biol Chem* 283: 31968–31980, 2008.
14. **Francini F, Bencini C, Piperio C, Squecco R.** Separation of charge movement components in mammalian skeletal muscle fibres. *J Physiol* 537: 45–56, 2001.
15. **Francini F, Bencini C, Squecco R.** Activation of L-type calcium channel in twitch skeletal muscle fibres of the frog. *J Physiol* 494: 121–140, 1996.
16. **Franzini-Armstrong C.** The membrane system of muscle cells. In: *Myology*. MacGraw-Hill, 2004, p. 232–256.
17. **Franzini-Armstrong C.** Unraveling the ryanodine receptor. *Biophys J* 67: 2135–2136, 1994.
18. **Fukuzawa A, Idowu S, Gautel M.** Complete human gene structure of obscurin: implications for isoform generation by differential splicing. *J Muscle Res Cell Motil* 26: 427–434, 2005.
19. **Fukuzawa A, Lange S, Holt M, Vihola A, Carmignac V, Ferreiro A, Udd B, Gautel M.** Interactions with titin and myomesin target obscurin and obscurin-like 1 to the M-band: implications for hereditary myopathies. *J Cell Sci* 121: 1841–1851, 2008.
20. **Gallagher PG, Forget BG.** An alternate promoter directs expression of a truncated, muscle-specific isoform of the human ankyrin 1 gene. *J Biol Chem* 273: 1339–1348, 1998.
21. **Gallagher PG, Tse WT, Scarpa AL, Lux SE, Forget BG.** Structure and organization of the human ankyrin-1 gene. Basis for complexity of pre-mRNA processing. *J Biol Chem* 272: 19220–19228, 1997.
22. **Giacomello E, Sorrentino V.** Localization of ank1.5 in the sarcoplasmic reticulum precedes that of SERCA and RyR: relationship with the organization of obscurin in developing sarcomeres. *Histochem Cell Biol* 131: 371–382, 2009.
23. **Giannini G, Conti A, Mammarella S, Scrobogna M, Sorrentino V.** The ryanodine receptor/calcium channel genes are widely and differentially expressed in murine brain and peripheral tissues. *J Cell Biol* 128: 893–904, 1995.
24. **Gokhin DS, Fowler VM.** Cytoplasmic gamma-actin and tropomodulin isoforms link to the sarcoplasmic reticulum in skeletal muscle fibers. *J Cell Biol* 194: 105–120, 2011.
25. **Hopitzan AA, Baines AJ, Kordeli E.** Molecular evolution of ankyrin: gain of function in vertebrates by acquisition of an obscurin/titin-binding-related domain. *Mol Biol Evol* 23: 46–55, 2006.
26. **Kontrogianni-Konstantopoulos A, Catino DH, Strong JC, Sutter S, Borisov AB, Pumplin DW, Russell MW, Bloch RJ.** Obscurin modulates the assembly and organization of sarcomeres and the sarcoplasmic reticulum. *FASEB J* 20: 2102–2111, 2006.
27. **Kontrogianni-Konstantopoulos A, Jones EM, Van Rossum DB, Bloch RJ.** Obscurin is a ligand for small ankyrin 1 in skeletal muscle. *Mol Biol Cell* 14: 1138–1148, 2003.
28. **Lange S, Ouyang K, Meyer G, Cui L, Cheng H, Lieber RL, Chen J.** Obscurin determines the architecture of the longitudinal sarcoplasmic reticulum. *J Cell Sci* 122: 2640–2650, 2009.
29. **Loud AV, Barany WC, Pack BA.** Quantitative evaluation of cytoplasmic structures in electron micrographs. *Lab Invest* 14: 996–1008, 1965.
30. **Maiweilidan Y, Klauza I, Kordeli E.** Novel interactions of ankyrins-G at the costameres: the muscle-specific Obscurin/Titin-Binding-related Domain (OTBD) binds plectin and filamin C. *Exp Cell Res* 317: 724–736, 2011.
31. **Melzer W, Schneider MF, Simon BJ, Szucs G.** Intramembrane charge movement and calcium release in frog skeletal muscle. *J Physiol* 373: 481–511, 1986.
32. **Mobley BA, Eisenberg BR.** Sizes of components in frog skeletal muscle measured by methods of stereology. *J Gen Physiol* 66: 31–45, 1975.
33. **Murphy RM, Larkins NT, Mollica JP, Beard NA, Lamb GD.** Calsequestrin content and SERCA determine normal and maximal Ca^{2+} storage levels in sarcoplasmic reticulum of fast- and slow-twitch fibres of rat. *J Physiol* 587: 443–460, 2009.
34. **Paolini C, Quarta M, Nori A, Boncompagni S, Canato M, Volpe P, Allen PD, Reggiani C, Protasi F.** Reorganized stores and impaired calcium handling in skeletal muscle of mice lacking calsequestrin-1. *J Physiol* 583: 767–784, 2007.
35. **Prosser BL, Hernandez-Ochoa EO, Zimmer DB, Schneider MF.** The Qgamma component of intra-membrane charge movement is present in mammalian muscle fibres, but suppressed in the absence of S100A1. *J Physiol* 587: 4523–4541, 2009.
36. **Randazzo D, Giacomello E, Lorenzini S, Rossi D, Pierantozzi E, Blaauw B, Reggiani C, Lange S, Peter AK, Chen J, Sorrentino V.** Obscurin is required for ankyrinB-dependent dystrophin localization and sarcolemma integrity. *J Cell Biol* 200: 523–536, 2013.
37. **Rios E, Pizarro G.** Voltage sensor of excitation-contraction coupling in skeletal muscle. *Physiol Rev* 71: 849–908, 1991.
38. **Rossi D, Barone V, Giacomello E, Cusimano V, Sorrentino V.** The sarcoplasmic reticulum: an organized patchwork of specialized domains. *Traffic* 9: 1044–1049, 2008.
39. **Rossi D, Bencini C, Maritati M, Benini F, Lorenzini S, Pierantozzi E, Scarcella AM, Paolini C, Protasi F, Sorrentino V.** Distinct regions of triadin are required for targeting and retention at the junctional domain of the sarcoplasmic reticulum. *Biochem J* 458: 407–417, 2014.
40. **Sambrook J, Russell DW.** *Molecular Cloning. A Laboratory Manual*. Cold Spring Harbor, NY: Cold Spring Harbor Laboratory, 2001.
41. **Sassoli C, Formigli L, Bini F, Tani A, Squecco R, Battistini C, Zecchi-Orlandini S, Francini F, Meacci E.** Effects of S1P on skeletal muscle repair/regeneration during eccentric contraction. *J Cell Mol Med* 15: 2498–2511, 2011.
42. **Sbrana F, Sassoli C, Meacci E, Nosi D, Squecco R, Paternostro F, Tiribilli B, Zecchi-Orlandini S, Francini F, Formigli L.** Role for stress fiber contraction in surface tension development and stretch-activated channel regulation in C2C12 myoblasts. *Am J Physiol Cell Physiol* 295: C160–C172, 2008.
43. **Schiaffino S.** Tubular aggregates in skeletal muscle: just a special type of protein aggregates? *Neuromuscul Disord* 22: 199–207, 2012.
44. **Schneider MF.** Control of calcium release in functioning skeletal muscle fibers. *Annu Rev Physiol* 56: 463–484, 1994.
45. **Sorrentino V.** Sarcoplasmic reticulum: structural determinants and protein dynamics. *Int J Biochem Cell Biol* 43: 1075–1078, 2011.
46. **Straub V, Rafael JA, Chamberlain JS, Campbell KP.** Animal models for muscular dystrophy show different patterns of sarcolemmal disruption. *J Cell Biol* 139: 375–385, 1997.
47. **Tybulewicz VL, Crawford CE, Jackson PK, Bronson RT, Mulligan RC.** Neonatal lethality and lymphopenia in mice with a homozygous disruption of the c-abl proto-oncogene. *Cell* 65: 1153–1163, 1991.
48. **Wu KD, Lytton J.** Molecular cloning and quantification of sarcoplasmic reticulum Ca^{2+}-ATPase isoforms in rat muscles. *Am J Physiol Cell Physiol* 264: C333–C341, 1993.
49. **Young P, Ehler E, Gautel M.** Obscurin, a giant sarcomeric Rho guanine nucleotide exchange factor protein involved in sarcomere assembly. *J Cell Biol* 154: 123–136, 2001.
50. **Zhou D, Birkenmeier CS, Williams MW, Sharp JJ, Barker JE, Bloch RJ.** Small, membrane-bound, alternatively spliced forms of ankyrin 1 associated with the sarcoplasmic reticulum of mammalian skeletal muscle. *J Cell Biol* 136: 621–631, 1997.